Inter-comparison of multiple two-way coupled meteorology and air quality models (WRF v4.1.1-CMAQ v5.3.1, WRF-Chem v4.1.1, and WRF v3.7.1-CHIMERE v2020r1) in eastern China

Chao Gao[1, 2], Xuelei Zhang[1, 2, *]Aijun Xiu[1, 2, *], Qingqing Tong[1, 2], Hongmei Zhao[1, 2], Shichun Zhang[1, 2], Guangyi Yang[1, 2, 3], Mengduo Zhang[1, 2, 3], and Shengjin Xie[1, 2, 4]

[1]Key Laboratory of Wetland Ecology and Environment, Northeast Institute of Geography and Agroecology, Chinese Academy of Sciences, Changchun, 130102, China

[2]Key Laboratory of Wetland Ecology and Environment, State Key Laboratory of Black Soils Conservation and Utilization, Northeast Institute of Geography and Agroecology, Chinese Academy of Sciences, Changchun, 130102, China

[3]University of Chinese Academy of Sciences, Beijing, 100049, China

[4]School of Environment, Harbin Institute of Technology, 150000, Harbin, China

Correspondence to: X.L. Zhang (zhangxuelei@iga.ac.cn) & A.J. Xiu (xiuaijun@iga.ac.cn)

Abstract

In the eastern China region, two-way coupled meteorology and air quality models have been applied aiming to more realistically simulate meteorology and air quality by accounting for the aerosol–radiation–cloud interactions. There have been numerous related studies being conducted, but the performances of multiple two-way coupled models simulating meteorology and air quality have not been compared in this region. In this study, we systematically evaluated annual and seasonal meteorological and air quality variables simulated by three open-source and widely used two-way coupled models (i.e., WRF-CMAQ, WRF-Chem, and WRF-CHIMERE) by validating the model results with surface and satellite observations for eastern China during 2017. Note that although we have done our best to keep the same configurations, this study is not aiming to screen which model is better or worse since different setups are still presented in simulations. Our evaluation results showed that all three two-way coupled models reasonably well simulated the annual spatiotemporal distributions of meteorological and air quality variables. The impacts of aerosol-cloud interaction (ACI) on model performances' improvements were limited compared to aerosol-radiation interaction (ARI), and several possible improvements on ACI representations in two-way coupled models are further discussed and proposed. When sufficient computational resources become available, two-way coupled models should be applied for more accurate air quality forecast and timely warning of heavy air pollution events in atmospheric environmental management. The potential improvements of two-way coupled models are proposed in future research perspectives.

1 Introduction

Aerosols in the atmosphere due to anthropogenic and nature emissions not only cause air pollution but also induce climate and meteorological impacts through aerosol-radiation interaction (ARI) and aerosol-cloud interaction (ACI) (Carslaw et al., 2010; Rosenfeld et al., 2014; Fan et al., 2016; IPCC, 2021). The feedbacks of aerosols to meteorology have been widely investigated by two-way coupled meteorology and air quality models in the past two decades (Jacobson, *1994, 1997, 1998, 2001,* 2002; Grell et al., 2005; Wong et al., 2012; Wang et al., 2014; Zhou et al., 2016; Briant et al., 2017; Feng et al., 2021). In these models, two-way interactions between meteorology and aerosols are enabled by including all the processes involving ARI or/and ACI (Grell and Baklanov, 2011; Wang et al., 2014; Briant et al., 2017; Wang et al., 2021). The fundamental theories, modeling technics, developments, and applications of two-way coupled meteorology and air quality models in North America, Europe and Asia have been systemically reviewed (Zhang, 2008; Baklanov et al., 2014; Gao et al., 2022).

As pointed out by these review papers, the treatments and parameterization schemes of all the physiochemical processes involving ARI and ACI can be very different in two-way coupled models, so that the simulation results from these models could vary in many aspects. At the same time, the configurations of coupled models, such as meteorological and chemical initial and boundary conditions (ICs and BCs), horizontal and vertical resolutions, and emission inventories and processing tools, etc., play important roles in models' simulations. In the past, model inter-comparison projects have been carried out targeting various two-way coupled meteorology and air quality models. For example, the Air Quality Model Evaluation International Initiative Phase II focused on the performance of multiple two-way coupled models and the effects of aerosol feedbacks in Europe and the United States (Brunner et al., 2015; Im et al., 2015a, b; Makar et al., 2015a, b). In Asia, the Model Inter-Comparison Study for Asia Phase III was conducted to evaluate ozone (O_3) and other gaseous pollutants, fine particular matter ($PM_{2.5}$), and acid and reactive nitrogen deposition with various models with/out ARI or/and ACI (Li et al., 2019; Chen et al., 2019; Itahashi et al., 2020; Ge et al. al., 2020; Kong et al., 2020). With respect to this project, Gao et al. (2018, 2020) have reviewed in detail the model performance of seven two-way coupled models from different research groups in simulating a heavy air pollution episode during January 2010 in North China Plain and how aerosol feedbacks affected simulations of meteorological variables and $PM_{2.5}$ concentrations. Targeting the heavy polluted India region, Govardhan et al. (2016) compared aerosol optical depth (AOD) and various aerosol species (black carbon, mineral dust, and sea salt) modeled by WRF-Chem (with ARI) and Spectral Radiation-Transport Model for Aerosol Species (with both ARI and ACI), but under different model configurations.

So far, there is no comprehensive comparisons of multiple coupled models under the same model configuration with respect to the high aerosol loading region over eastern China, where has experienced rapid growth of economy, urbanization, population, as well as severe air quality problems in the past decades (He et al., 2002; Wang and Hao, 2012; Gao et al., 2017; Geng et al., 2021). In the eastern China region (ECR), several open-source and proprietary two-way coupled models have been applied to investigate the ARI and/or ACI effects, yet most studies have focused on certain short-term episodes of heavy air pollution without any year-long simulations (Xing et al., 2017; Ding et al., 2019; Ma et al., 2021). The commonly used open-source models in ECR are WRF-Chem and WRF-CMAQ (Grell et al., 2005; Wong et al., 2012), but there is no any application of the two-way coupled WRF-CHIMERE model that has been applied to examine aerosol-radiation-cloud interactions in Europe and Africa (Briant et al., 2017; Tuccella et al., 2019). At the same time, model simulations should be compared not only against surface measurement data but also satellite data (Zhao et al., 2017; Hong et al., 2017; Campbell et al., 2017; Wang et al., 2018). Even though the running time of an individual modeling system (e.g., WRF-CMAQ and WRF-CHIMERE) was evaluated by considering its online and offline versions and under various computing configurations (Wong et al., 2012; Briant et al., 2017), the computational efficiencies of multiple two-way coupled models need to be accessed under the same computing conditions as well.

In this paper, a comparative evaluation of three open-sourced two-way coupled meteorology and air quality models (WRF-CMAQ, WRF-Chem and WRF-CHIMERE) in ECR is conducted. The remainder of the paper is organized as follows: Section 2 describes the study methods including model configurations and evaluation protocols. Sections 3 and 4 presents the analyses and intercomparisons of simulations from these three two-way coupled models with regard to meteorology and air quality, respectively. The major findings of this work are summarized in Section 5.

2 Data and methods

2.1 Model configurations and data sources

One-year long-term simulations in eastern China were examined using the two-way coupled WRF-CMAQ, WRF-Chem, and WRF-CHIMERE models, with and without enabling ARI and/or ACI, and with 27-km horizontal grid spacing (there were 110, 120, and 120 grid cells in the east–west direction, and 150, 160, and 170 in the north–south direction for WRF-CMAQ, WRF-Chem, and WRF-CHIMERE, respectively). *All the three coupled models used in this study have 30 levels* (i.e., 29 layers) *from the surface to 100 hPa with 11 layers in the bottom 1 km and the bottom-layer thickness being 23.2 m.* The anthropogenic emissions of Multi-resolution Emission Inventory for China (MEIC) (Li et al., 2017) and the Fire INventory from NCAR verision 1.5 (FINN v1.5) biomass burning emissions (Wiedinmyer et al., 2011) were applied in our simulations, and their spatial, temporal, and species allocations were performed using Python language (Wang et al., 2023). Biogenic emissions were calculated using the Model of Emissions of Gases and Aerosols from Nature version 3.0 (MEGAN v3.0) (Gao et al., 2019). Dust and sea-salt emissions were both used with calculations of inline modules, as shown in Table 1. *The meteorological ICs and lateral BCs were derived from the National Center for Environmental Prediction Final Analysis (NCEP-FNL) datasets (http://rda.ucar.edu/datasets/ds083.2), with a horizontal resolution of 1° × 1° at 6-hour intervals for each of the three coupled models, and the flux in model-top boundary is set zero*. To improve the long-term accuracy of meteorological variables when using the WRF model, options of observational and grid four-dimensional data assimilation (FDDA) were turned on, and pressure, station height, relative humidity, wind speed, and wind direction were observed four times per day at 00:00, 06:00, 12:00, and 18:00 UTC from 2168 stations (https://doi.org/10.5281/zenodo.6975602, Gao et al., 2022). *Turing on FDDA in two-way coupled models could dampen the simulated aerosol feedbacks (Wong et al., 2012; Forkel et al., 2012; Hogrefe et al., 2015; Zhang et al., 2016). To reduce the effects of enabling FDDA on aerosol feedbacks in long-term simulations, here the nudging coefficients for u/v wind, temperature, and water vapor mixing ratio above the planetary boundary layer were set to 0.0001* s^{-1}*, 0.0001* s^{-1}*, and 0.00001* s^{-1}*, respectively. The chemical ICs/lateral BCs were downscaled from the Whole Atmosphere Community Climate Model (WACCM) for WRF-CMAQ and WRF-Chem via the mozart2camx and mozbc tools, respectively. WRF-CHIMERE used the climatology from a general circulation model developed at the Laboratoire de Météorologie Dynamique (LMDz) coupling a global chemistry and aerosol model INteractions between Chemistry and Aerosols (INCA) (Mailler et al., 2017). For chemical model-top BCs, WRF-CMAQ and WRF-Chem models both take into account the impacts of stratosphere-troposphere* O_3 *exchange using the parameterization of* O_3*-potential vorticity (Safieddine et al., 2014; Xing et al., 2016), the related options for the two models were used in this study. In WRF-CHIMERE, the climatology from LMDz-INCA data was utilized (Mailler et al., 2017)*.

The options of parameterization schemes of aerosol–radiation–cloud interactions are listed in Table 1. *To keep the consistency of physical schemes, the same RRTMG shortwave and longwave radiation schemes and Morrison microphysics schemes are adopted in both WRF-Chem and WRF-CMAQ. WRF-CHIMERE applied the same radiation schemes and Thompson microphysics scheme. The different other schemes (cumulus, surface, and land surface) in WRF-CMAQ and WRF-Chem were chosen according to widely used options outlined in Table S1 of Gao et al. (2022). The other schemes used in WRF-CHIMERE are the same as with WRF-Chem. To consider the effects of clouds on radiative transfer calculations, the fractional cloud cover and cloud optical properties were included in the RRTMG shortwave/longwave radiation schemes used by all three coupled models (Xu and Randall, 1996; Iacono et al., 2008). The coupled WRF-CMAQ model with the Kain-Fritsch cumulus scheme included the cumulus cloud fraction impacts on RRTMG radiation (Alapaty et al., 2012), but not the WRF-Chem and WRF-CHIMERE models with the Grell-Freitas cumulus scheme. In the Fast-JX photolysis scheme used by the three coupled models, the impacts of clouds are included by considering cloud cover and cloud optical properties. However, the calculations of cloud cover and cloud optical properties are different in these models and all the relevant information is listed in Table S1. As illustrated in Tables 1 and S2 for aerosol size distribution, we used modal approach with Aitken, accumulation and coarse modes in WRF-CMAQ, and the 4-bin and 10-bin sectional approaches in WRF-Chem and WRF-CHIMERE models, respectively (Binkowski and Roselle, 2003; Zaveri et al., 2008; Nicholls et al., 2014; Menut et al., 2013, 2016).*

To demonstrate the capabilities of the three two-way coupled models with/without feedbacks in simulating meteorology and air quality, we undertook comprehensive evaluations of the strengths and weaknesses each coupled model, validated against extensive ground-based and satellite measurements. Ground-based data included 572 hourly ground-based meteorological observations (air temperature (T2) and relative humidity (RH2) air temperature at 2m above the surface, wind speed at 10m above the surface (WS10), and precipitation (PREC)) (http://data.cma.cn), 327 hourly national environmental observations (fine particulate matter ($PM_{2.5}$), ozone (O_3), nitrogen dioxide (NO_2), sulfur dioxide (SO_2), and carbon monoxide (CO)) (http://106.37.208.233:20035), 109 hourly surface shortwave radiation (SSR) measurements (Tang et al., 2019) and 74 radiosonde sites retrieved twice per day (Guo et al., 2019); the locations of these data are depicted in Fig. 1. Because there were no observed water vapor mixing ratio (w) data, this parameter was calculated via the formula $w = \frac{rh}{w_s}$, where rh is the relative humidity and w_s is the saturation mixing ratio (Wallace and Hobbs, 2006).

Satellite data included the following: monthly average downwelling short-/long-wave flux at the surface and short-/long-wave flux at the top of the atmosphere (TOA) from the Clouds and the Earth's Radiant Energy System (CERES) (https://ceres.larc.nasa.gov); precipitation from the Tropical Rainfall Measuring Mission (TRMM); cloud fraction, liquid water path (LWP), and aerosol optical depth (AOD) from the Moderate Resolution Imaging Spectroradiometer (MODIS); tropospheric NO_2 column and SO_2 column in the planetary boundary layer (PBL) from the Ozone Monitoring Instrument (OMI); total CO column from the Measurements of Pollution in the Troposphere (MOPITT) (https://giovanni.gsfc.nasa.gov/giovanni); total column ozone (TCO) from the Infrared Atmospheric Sounding Interferometer-Meteorological Operational Satellite-A (IASI-METOP-A) (https://cds.climate.copernicus.eu/cdsapp#!/dataset/satellite-ozone?tab=form); and total ammonia (NH_3) column from IASI-METOP-B (https://cds-espri.ipsl.fr/iasibl3/iasi_nh3/V3.1.0). These data were downloaded and interpolated to the same horizontal resolution as the model results using Rasterio library (Gillies et al., 2013), then the model and observed values at each grid point were extracted.

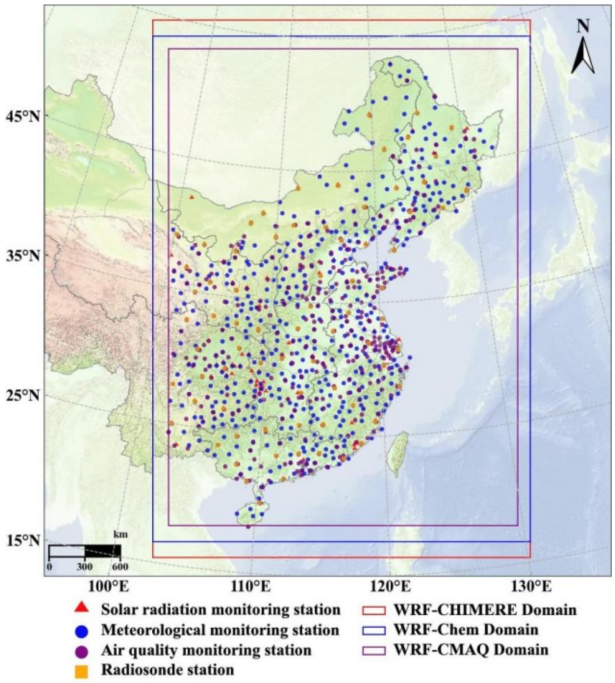

Figure 1. Modeling domains (WRF-CMAQ, WRF-Chem, and WRF-CHIMERE), and solar radiation, meteorology, air quality, and radiosonde stations.

Table 1. Model setups and inputs for the two-way coupled models (WRF-CMAQ, WRF-Chem and WRF-CHIMERE).

		WRF-CMAQ	WRF-Chem	WRF-CHIMERE
Domain configuration	Horizontal grid spacing	27 km (110 × 150)	27 km (120 × 160)	27 km (120 × 170)
	Vertical resolution	*30 levels*	*30 levels*	*30 levels*
Physics parameterization	Shortwave radiation	RRTMG	RRTMG	RRTMG
	Longwave radiation	RRTMG	RRTMG	RRTMG
	Cloud microphysics	Morrison	Morrison	Thompson
	PBL	ACM2	YSU	YSU
	Cumulus	Kain-Fritsch	Grell-Freitas	Grell-Freitas
	Surface	Pleim-Xiu	Monin-Obukhov	Monin-Obukhov
	Land surface	Pleim-Xiu LSM	Noah LSM	Noah LSM
	Icloud	*Xu-Randall method*	*Xu-Randall method*	*Xu-Randall method*
Chemistry scheme	*Aerosol mechanism*	*AERO6*	*MOSAIC*	*SAM*
	Aerosol size distribution	*Modal (3 modes)*	*Sectional (4 bins)*	*Sectional (10 bins)*
	Aerosol mixing state	Core-Shell	Core-Shell	Core-Shell
	Gas-phase chemistry	CB6	CBMZ	MELCHIOR2
	Photolysis	*Fast-JX with cloud effects*	*Fast-JX with cloud effects*	*Fast-JX with cloud effects*
Emission	Anthropogenic emission	MEIC 2017	MEIC 2017	MEIC 2017
	Biogenic emission	MEGAN v3.0	MEGAN v3.0	MEGAN v3.0
	Biomass burning emission	FINN v1.5	FINN v1.5	FINN v1.5
	Dust emission	Foroutan	GOCART	Menut
	Sea-salt emission	Gong	Gong	Monahan
Input data	Meteorological ICs and BCs	FNL	FNL	FNL
	Chemical ICs and BCs	MOZART	MOZART	LMDZ-INCA

2.2 Scenario set up

To thoroughly assess the performance of WRF v4.1.1-CMAQ v5.3.1, WRF-Chem v4.1.1, and WRF v3.7.1-CHIMERE v2020r1 and its affected by aerosol feedbacks over eastern during 2017, eight sets of annual hindcast simulations with/without ARI and/or ACI were conducted, as presented in Table 2. *Compared to WRF v4.1.1-CMAQ v5.3.1 and WRF-Chem v4.1.1, this version of WRF v3.7.1-CHIMERE v2020r1 can be officially obtained and the higher version of WRF-CHIMERE has not been developed.* It should be noted that the officially released WRF-Chem and WRF-CHIMERE are capable of simulating ARI and ACI, but WRF-CMAQ is not. In all of the simulations performed in this study, a month of spin-up time was set up to reduce the influence of the initial conditions. Multiple statistical metrics between each scenario simulation and ground-based/satellite-borne observations were used including the correlation coefficient (R), mean bias (MB), normalized mean bias (NMB), *normalized gross error (NGE)*, and root mean square error (RMSE). The mathematical definitions of these metrics are provided in Supplement S1. *To compare simulations by three coupled models, the respective model configurations of physics and chemistry routines are set as consistent as possible.* We systemically analyzed the annual and seasonal statistical metrics of meteorological and air quality variables including simulations by all three two-way coupled models with/without enabling ARI and/or ACI effects. We then quantified the respective contributions of the ARI and ACI effects to model performance.

Table 2. Summary of scenarios setting in three coupled models.

Model	Scenario	Configuration option	Description
WRF-CMAQ	(1) WRF-CMAQ_NO	DO_SW_CAL=F	Without aerosol feedbacks
	(2) WRF-CMAQ_ARI	DO_SW_CAL=T	ARI
WRF-Chem	(3) WRF-Chem_NO	aer_ra_feedback=0 wetscav_onoff=0 cldchem_onoff=0	Without aerosol feedbacks
	(4) WRF-Chem_ARI	aer_ra_feedback=1 wetscav_onoff=0 cldchem_onoff=0	ARI
	(5) WRF-Chem_BOTH	aer_ra_feedback=1 wetscav_onoff=1 cldchem_onoff=1	ARI and ACI
WRF-CHIMERE	(6) WRF-CHIMERE_NO	direct_feed_chimere=0 indirect_feed_chimere=0	Without aerosol feedbacks
	(7) WRF-CHIMERE_ARI	direct_feed_chimere=1 indirect_feed_chimere=0	ARI
	(8) WRF-CHIMERE_BOTH	direct_feed_chimere=1 indirect_feed_chimere=1	ARI and ACI

3 Multi-model meteorological evaluations

This section presents annual and seasonal (March–April–May, Spring; June–July–August, Summer; September–October–November, Autumn; and December–January–February, Winter) statistical metrics of simulated meteorological variables and air quality when compared with ground-based and satellite observations, as well as a discussion of the running times of the eight scenario simulations.

3.1 Ground-based observations

Figures 2 and S1–S7 illustrate the spatial distributions of R, MB, and RMSE for hourly SSR, T2, Q2, RH2, WS10, PREC, PBLH00, and PBLH12 from WRF-CMAQ, WRF-Chem, and WRF-CHIMERE with/without turning on aerosol feedbacks against ground-based observations from each site across the whole of 2017. The calculated annual model evaluation metrics for all sites in eastern China are summarized in Table S1, and the related seasonal R and MB values are presented in Fig. 3. *Here, we mainly focused on the comparisons of SSR, T2, RH2, and WS10, and the analysis of PREC, PBLH00, and PBLH12 are presented in Section 1.1 of Supplement.*

The accuracy of radiation predication is of great significance in evaluating ARI. Yearly and seasonal average simulated SSR data were compared with ground-based observations (*Figs. 3 – 4* and Table S3), and SSR over eastern China was simulated reasonably well by all models with R values in the range of 0.61–0.78. *All simulated results were overestimated at both annual and seasonal scales (MBs in spring and summer were larger than those in autumn and winter).* The overestimations of annual SSR were 19.98, 14.48, and 9.24 W m^{-2} for WRF-CMAQ, WRF-Chem, and WRF-CHIMERE, respectively. Overestimations of SSR by most two-way coupled models were also reported for Europe and North America in the comparative study conducted by Brunner et al. (2015). Such overestimations could be explained by multiple factors, namely, the uncertainties in cloud development owing to PBL and convection parameterizations (Alapaty et al., 2012), and the diversity in treatment of land surface processes (Brunner et al., 2015), which appear to play more important roles than does the enabling of two-way aerosol feedbacks on SSR through ARI and ACI effects in the models. When the three models considered ARI effects, the simulation accuracy of SSR, over both the whole year and in the four seasons were improved, but the enabling of ACI effects resulted in relatively limited improvement. In addition, the MB variations of WRF-CMAQ and WRF-Chem simulations were higher in spring and winter than those in summer and autumn, while the MB of WRF-CHIMERE simulations showed a maximum in summer (−10.33 W m^{-2}) and minimum in autumn (−7.64 W m^{-2}). Both the annual and seasonal reductions in SSR simulated by WRF-Chem and WRF-CHIMERE with ACI effects enabled were much smaller than those with ARI effects enabled.

In general, the simulated magnitudes and temporal variations of air temperature at 2 m above the ground showed a high order of consistency with observations (R = 0.88–0.97). *Looking at annual and seasonal T2, models tended to have a negative bias, and T2 underestimations in spring and winter were greater than those in summer and autumn (Figs. 3 and 4).* As pointed out by Makar et al. (2015a), WRF-CHEM and GEM-MACH gave negative MBs in summer and positive MBs in winter when both ACI and ARI effects were enabled, and WRF-CMAQ with only ARI effects enabled also produced negative MBs in summer over North America during 2010; note that the Makar et al (2015a) study lacked evaluations of meteorology in winter using WRF-CMAQ. The comparison results of MBs indicated that WRF-CHIMERE > WRF-CMAQ > WRF-Chem. The annual and seasonal MBs of WRF-CMAQ and WRF-Chem were approximately −1 °C, while those of WRF-CHIMERE ranged from −2 to −1 °C. The RMSEs were approximately equal for WRF-CMAQ (2.71–3.05 °C) and WRF-Chem (2.82–3.27 °C), and larger for WRF-CHIMERE (3.39–4.53 °C) at both annual and seasonal scales. It is noteworthy that underestimations of annual and seasonal T2 were mitigated in eastern China in the three coupled models when ARI effects were enabled. When ACI effects were enabled, the MBs for T2 simulated by WRF-Chem_BOTH showed no significant changes compared with those of WRF-Chem_NO; WRF-CHIMERE_BOTH further enhanced the underestimations of T2 in the full year (−1.30 °C), spring (−0.12 °C), and winter (−0.40 °C) compared with WRF-CHIMERE_NO.

Looking at RH2, annual and seasonal simulations using WRF-CMAQ had the highest correlation with the observed values, followed by WRF-Chem, and WRF-CHIMERE, and the smallest correlation coefficients for all three models occurred in autumn (~ 0.5). The spatial MBs between simulations by the three models and observations showed a general converse trend compared with T2 (i.e., RH2 was overestimated where T2 was underestimated, and vice versa). This can be explained by the calculation of RH2 being based on T2 in the models (Wang et al., 2021). The annual and seasonal MBs were approximately 0.65%–71.03% and −21.30% to 60.00%, respectively (Fig. 4 and Table S3), and only WRF-Chem produced negative MBs in summer. The magnitude of RMSE showed an inverse pattern compared with R for all three models, with maximum (28.48%–29.52%) and minimum (12.57%–16.07%) values shown in autumn and summer, respectively. *As shown in Figs. 3–4 and Table S3, WRF-CMAQ_ARI further reduced the overestimations of annual and seasonal RH2 in eastern China, while WRF-Chem_ARI (except for summer) and WRF-CHIMERE_ARI showed the opposite trend.* Moreover, variations in annual and seasonal RH2 MBs simulated by WRF-Chem_BOTH and WRF-CHIMERE_BOTH were further reduced compared with WRF-Chem_ARI (except for summer) and WRF-CHIMERE_ARI, respectively.

Similar analyses were also performed for WS10, and revealed that WRF-CMAQ performed better in capturing WS10 patterns compared with WRF-Chem and WRF-CHIMERE. *The R values for all three models ranged from 0.47 to 0.60; WRF-CMAQ and WRF-Chem overestimated wind speed by approximately 0.5 m s^{-1}, while WRF-CHIMERE overestimated it by approximately 1.0 m s^{-1} (Table S3 and Figs. 3–4)*. The overestimation of WS10 under real-world low wind conditions is a common phenomenon of current weather models, which is mainly caused by outdated geographic data, coarse model resolution, and a lack of a good physical representation of the urban canopy (Gao et al., 2015, 2018). All three models presented lower correlations (0.31–0.54) and MBs (0.20–0.86 m s^{-1}) in summer compared with other seasons, and the RMSEs were approximately 2.0 m s^{-1}. When ARI effects were enabled, the overestimations of the three models were alleviated, especially for WRF-CMAQ_ARI.

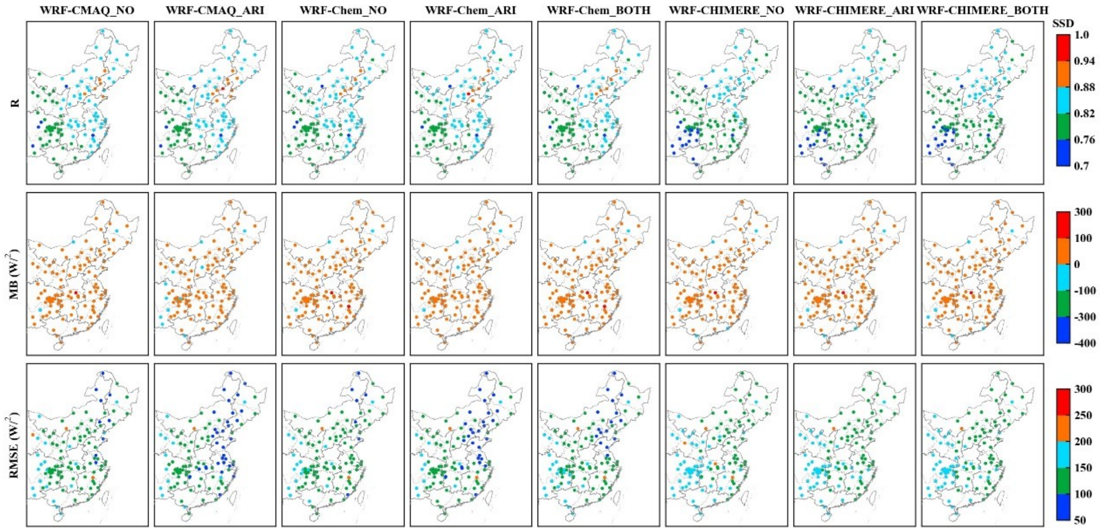

Figure 2. Statistical metrics (R, MB, and RMSE) between annual simulations and observations of surface shortwave radiation in eastern China.

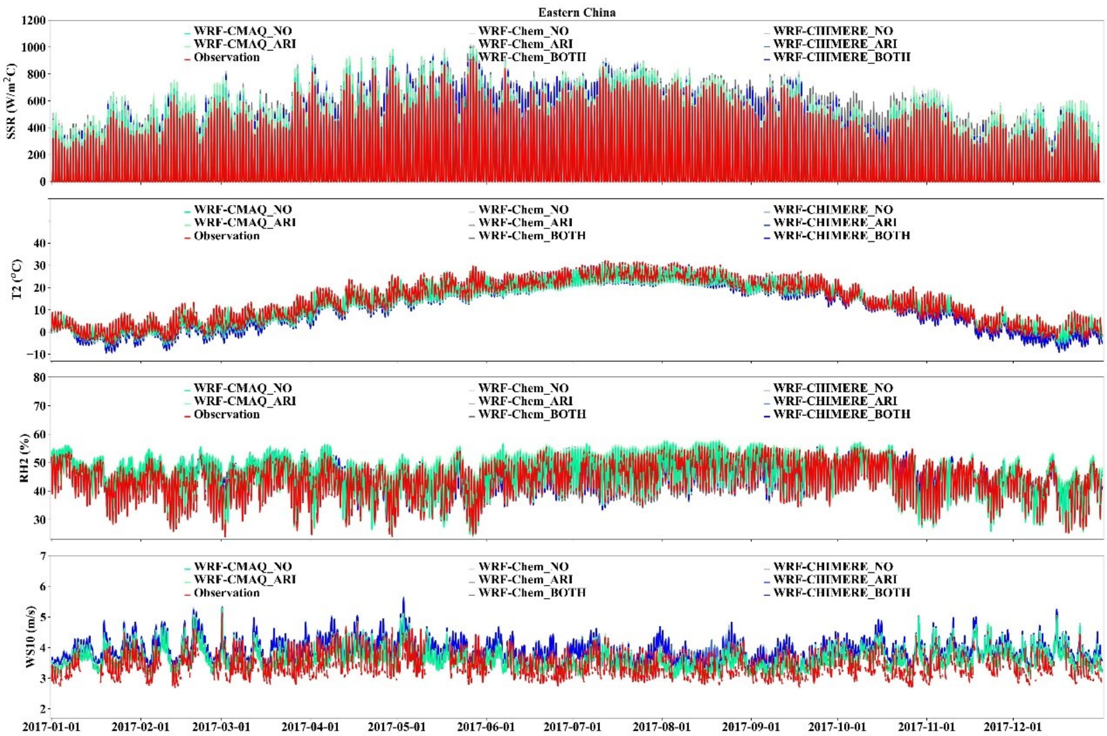

Figure 3. Time series of observed and simulated hourly SSR, T2, RH2 and WS10 by coupled WRF-CMAQ, WRF-Chem and WRF-CHIMERE with/without aerosol feedbacks over Eastern China during the year of 2017.

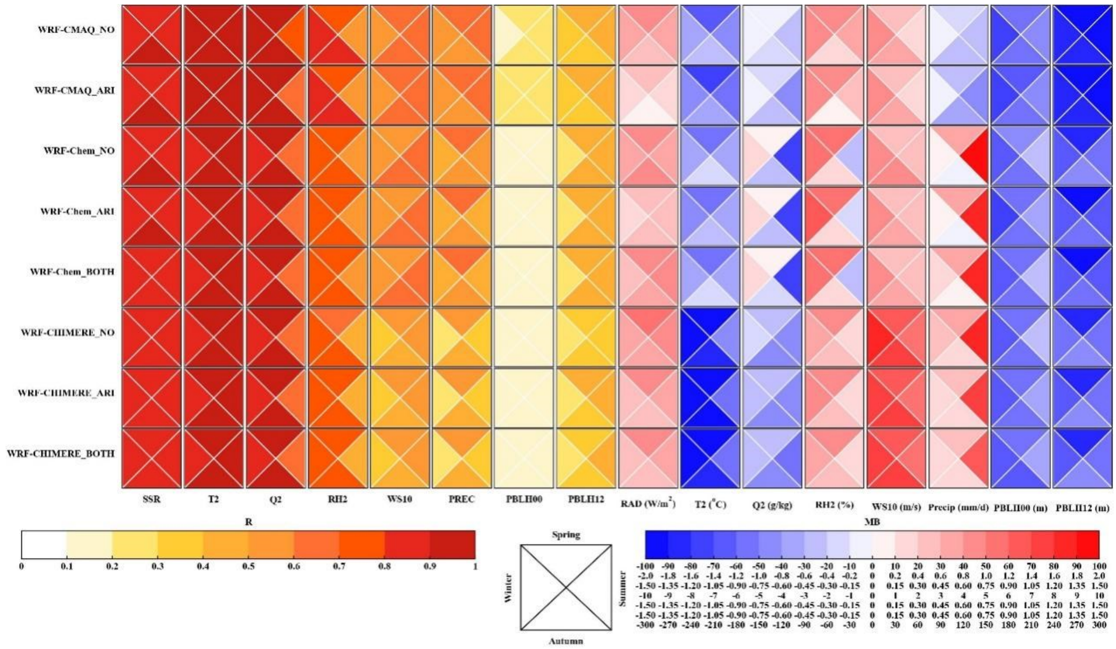

Figure 4. Portrait plots of statistical indices (R and MB) between seasonal simulations and surface observations of meteorological variables (SSR, T2, Q2, RH2, WS10, PREC, and PBLH at LT 08:00 and 20:00) in eastern China.

To identify and quantify how well our results compare with previous studies using two-way coupled models, we here discuss comparisons between our work and earlier research in terms of the evaluation results of meteorology and air quality; meteorology is discussed in this section and air quality is discussed in Section 4.1. Box-and-whisker plots were used and the 5th, 25th, 75th, and 95th percentiles were used as statistical indicators. In the plots, the dashed lines in the boxes are the mean values, and the circles represent outliers. Previous studies mainly used WRF-Chem and WRF-CMAQ to evaluate meteorology and air quality, while applications of WRF-NAQPMS and GRAPES-CUACE were scarce. As mentioned in Section 1, investigations of meteorology and air quality using WRF-CHIMERE with/without aerosol feedbacks have not previously been conducted in eastern China. Therefore, only evaluation results involving WRF-Chem and WRF-CMAQ to study aerosol feedbacks are analyzed herein.

The statistical metrics of T2, RH2, Q2, and WS10 in this study compared with the evaluation results of previous studies are presented in Fig. S8. According to the number of samples (NS) in the statistical metrics of each meteorological variable, most previous studies mainly involved the simulation and evaluation of T2, WS10, and RH2, with relatively few studies focusing on Q2. Compared with the evaluation results of previous studies, the ranges of statistical metrics in our study were roughly similar, but there were some important differences. The R values of the WRF-CMAQ and WRF-Chem models in our study were higher than those of previous studies; the MBs of T2 simulated via WRF-CMAQ were smaller, but those of T2 simulated via WRF-Chem were larger; and the RMSEs of the WRF-CMAQ simulation were larger, but those of the WRF-Chem simulation were smaller. For RH2, the R values for WRF-CMAQ and WRF-Chem in this study were all larger than the average level of previous studies, while the MBs and RMSEs for WRF-CMAQ were larger, and those for WRF-Chem were smaller than the average of previous studies. For Q2, the model performance of WRF-CMAQ in this study was generally better than the average level of previous studies, but the R between WRF-Chem simulation results and observed values was higher (and MB and RMSE were lower) than the average level of previous studies. We also conclude that the simulation results of WRF-CMAQ and WRF-Chem in our study better reproduced variations in WS10 compared with previous studies.

3.2 Satellite-borne observations

To further evaluate the performance of WRF-CMAQ, WRF-Chem, and WRF-CHIMERE against satellite observations, we analyzed the annual and seasonal statistical metrics of short- and long-wave radiation at the surface, precipitation, cloud cover, and liquid water path simulated by the three coupled models with and without aerosol feedbacks, via comparisons between simulations and satellite-borne observations (Table 3; Figures 5, S9, S12–S14). In addition, the evaluations of short- and long-wave radiation at top of the atmosphere (TOA) are presented in Section 1.2 of Supplement.

As shown in Table 3 and Fig. 5, the three coupled models showed relative poor performance for the shortwave radiation variables at the surface (SSR) annual MBs of 8.21–30.74 W m^{-2}, and correlations ranging from 0.61 to 0.78. A similar poor performance for shortwave radiation was also reported in the USA using the coupled WRF-CMAQ and offline WRF models (Wang et al., 2021). The overall seasonal characteristics of SSR were successfully reproduced by the three coupled models (Fig. S10). Meanwhile, no matter whether aerosol feedbacks were enabled or not, all three models overestimated seasonal SSR (except for WRF-Chem_ARI in winter), and showed higher MBs in spring and summer than in autumn and winter. The seasonal SSR overestimations may be a direct result of the underestimation of calculated AOD when considering ARI effects (Wang et al., 2021). Compared to SSR, the three coupled models predicted the longwave radiation variables at the surface (SLR) well (R values up to 0.99), with annual domain-average MBs of −9.97 to −6.05 W m^{-2}. Significant seasonal differences in simulated longwave radiation were also present among the three coupled models; all WRF-CMAQ and WRF-CHIMERE scenarios gave underestimations, with maximum and minimum values of SLR in winter and summer, respectively, while the maximum underestimations of WRF-Chem occurred in autumn, especially for WRF-Chem_BOTH (Fig. S9).

As all three coupled models adopted the same grid resolution (27 × 27 km) and short- and long-wave radiation schemes (RRTMG), the above analysis demonstrated that *the representation differences for aerosol components, size distributions and mechanisms contributed to the diversity of seasonal MBs (Tables 1 and S2).* Moreover, the three two-way coupled models with ARI feedbacks enabled effectively improved the performances of annual and seasonal SSR; however, for SLR, performance improvements were much more variable across the three coupled models and across different scenarios with and without ARI and/or ACI feedbacks enabled (Table S4). *When ARI effects are enabled, the diversities of refractive indices of aerosol species groups lead to the discrepancies of online calculated aerosol optical properties in* *different shortwave and longwave (SW and LW) bands in the RRTMG SW/LW radiation schemes of WRF-CMAQ, WRF-Chem, and WRF-CHIMERE (Tables S5–S6). The online calculated cloud optical properties induced by aerosol absorption in the RRTMG radiation schemes are different in treatments of aerosol species groups in the three coupled models. With enabling ACI effects, the activation of cloud droplets from aerosols based on the Köhler theory is taken into account in WRF-Chem and WRF-CHIMERE, in comparison to simulations without aerosol feedbacks (Table S7). The treatments of prognostic ice nucleating particles (INP) formed via heterogeneous nucleation of dust particles (diameters > 0.5 μm) and homogeneous freezing of hygroscopic aerosols (diameters > 0.1 μm) are only considered in WRF-CHIMERE, but the prognostic ice nucleating particles are not included in WRF-CMAQ and WRF-Chem. These discrepancies eventually contribute to the differences of simulated radiation changes caused by aerosols.*

From IPCC 2007 to IPCC 2021, the effects of aerosol feedbacks (especially for ACI effects) on precipitation and cloud processes remain under debate. Here, we further assessed annual and seasonal simulated precipitation, cloud cover, and liquid water pathways in eastern China with high aerosol loadings against satellite observations (Table 3 and Figs. S12–S14), and attempted to provide new insights from a yearly perspective into enabling online feedbacks in two-way coupled modeling simulations.

The results illustrated those correlations of precipitation via WRF-CMAQ (0.51–0.89) were larger than those of WRF-Chem (0.61–0.73) and WRF-CHIMERE (0.54–0.70). WRF-CMAQ had the best correlation in winter, while WRF-Chem and WRF-CHIMERE had the best correlation in spring; all three models showed their worst correlation in summer. The reason for this is that numerical models struggle to effectively capture enhanced convective activity in summer. Huang and Gao (2018) also pointed out that accurate representations of lateral boundaries are crucial in improving precipitation simulations during summer over China. WRF-CMAQ underestimated annual precipitation, with MBs of −76.49 to −51.93 mm, while WRF-Chem and WRF-CHIMERE produced large precipitation overestimations ranging from +108.04 to +207.05 mm (Table 3), especially in regions of southern China (Fig. S11). WRF-CMAQ also produced negative biases (−27.89 to +42.08 mm) of seasonal precipitation, excluding WRF-CMAQ_ARI in winter. WRF-Chem and WRF-CHIMERE only underestimated seasonal precipitation in autumn (−31.39 to −26.89 mm) and winter (−7.12 to −4.43 mm), respectively (Fig. S12). The variations in annual and seasonal MBs of precipitation were consistent with changes in cloud fraction and LWP (Zhang et al., 2016), which will be discussed in more detail below.

When aerosol feedbacks were considered, the ARI-induced reductions in the annual MBs of precipitation for WRF-CMAQ, WRF-Chem, and WRF-CHIMERE were 24.56, 12.11, and 4.70 mm, respectively. WRF-Chem_BOTH (24.9 mm) and WRF-CHIMERE_BOTH (3.41 mm) enhanced the overestimation of annual precipitation compared with WRF-Chem_ARI and WRF-CHIMERE_ARI, respectively. Significant increases (+53.15 mm) and decreases (−6.3 to −3.41 mm) in MBs in winter and summer, respectively, were produced by WRF-CMAQ and the other two models with ARI effects enabled compared with no feedbacks. WRF-Chem and WRF-CHIMERE with both ARI and ACI effects enabled led to larger enhancements of MBs (+3.54 to +7.46) at the seasonal scale (Fig. S12). It must be noted that the discrepancies in simulated precipitation could mainly be attributed to the selection of different microphysics and cumulus schemes in WRF-CMAQ (Morrison and Kain-Fritsch), WRF-Chem (Morrison and Grell-Freitas), and WRF-CHIMERE (Thompson and Grell-Freitas).

Cloud fraction (CF) and LWP can significantly influence the spatiotemporal distributions of precipitation; our simulated results of annual and seasonal CF over eastern China are presented in Table 3 and Fig. S13. Overall, WRF-CMAQ performed best in simulating CF. The R values for WRF-Chem during summer (0.69) and winter (0.70) were larger than those of WRF-CMAQ (0.59 and 0.64) and WRF-CHIMERE (0.56 and 0.66), while WRF-CMAQ and WRF-CHIMERE showed better simulation results in winter and autumn with correlations of up to 0.89 and 0.67, respectively. All three coupled models underestimated annual and seasonal CF with MBs that ranged from −16.83% to −6.18% and −21.13% to −4.13%, respectively; these were consistent with previous two-way coupled modeling studies using WRF-CMAQ (−19.7%) and WRF-Chem (−32% to −9%) in China (Hong et al., 2017; Zhao et al., 2017). All models reasonably simulated annual LWP in eastern China, with R values above 0.55 and negative biases varying from −57.36 to −31.29 g m^{-2}. The underestimations were closely related to missing cloud homogeneity (Wang et al., 2015; Dionne et al., 2020) and excessive conversion of liquid to ice in all selected cloud microphysics schemes (Klein et al., 2009). As shown in Fig. S14, all models showed their best performance in simulating LWP in spring (R = 0.51–0.79) and exhibited the largest underestimations in winter (MBs of −54.82 to −40.89 g m^{-2}), except for WRF-Chem, which had its maximum bias in autumn.

In terms of quantitatively determining the functions of aerosol feedbacks on CF and LWP, all simulated scenarios revealed that WRF-CMAQ_ARI overwhelmingly decreased annual and seasonal underestimations of CF (0.48%–1.05%) and LWP (3.03–4.29 g m^{-2}), while there were slightly increased underestimations (CF: 0.02%–0.39%; LWP: 0.03–0.58 g m^{-2}) in WRF-Chem_ARI and WRF-CHIMERE_ARI. Larger variations in annual and seasonal MBs of CF (0.23%–0.93%) and LWP (−2.96 g m^{-2} to 7.38 g m^{-2}) were produced by WRF-CHIMERE_BOTH compared with WRF-CHIMERE_ARI. WRF-Chem_BOTH showed equivalent variations (CF: 0.03%–0.71%; LWP: 0.02–2.89 g m^{-2}) to those of WRF-Chem_ARI. *This may be explained as the different parameterization treatments of cloud droplet number concentration (CDNC) simulated by the three coupled models with/without enabling ACI effects. The cloud condensation nuclei activated from aerosol particles can increase CDNC and impact on LWP and CF. Without enabling any aerosol feedbacks or only enabling ARI, the CDNC is default prescribed as a constant value of 250 cm^{-3} in the Morrison scheme of WRF-CMAQ and WRF-Chem and 300 cm^{-3} in the Thompson scheme of WRF-CHIMERE. When only ACI or both ARI and ACI are enabled, the online calculating of prognostic CDNC is performed in WRF-Chem and WRF-CHIMERE by using the method of maximum supersaturation (Abdul-Razzak and Ghan, 2002; Chapman et al., 2009; Tuccella et al., 2019).* Although we have obtained preliminary quantitative results of the ACI effects on regional precipitation, CF, and LWP, it should be kept in mind that several limitations in representing ACI effects still exist in state-of-the-art two-way coupled models; these include a lack of consideration of the responses of convective clouds to ACI (Tuccella et al., 2019), and a lack of numerical descriptions of giant cloud condensation nuclei (Wang et al., 2021) and heterogeneous ice nuclei (Keita et al., 2020).

Table 3. Statistical metrics (R, MB, NMB, NGE, and RMSE) between annual simulations and satellite retrievals of surface shortwave and longwave radiation, TOA shortwave and longwave radiation, precipitation, cloud fraction, and liquid water path in eastern China. The best results are in bold, while mean simulations and observations are in italics.

Variables	Statistics	WRF-CMAQ_NO	WRF-CMAQ_ARI	WRF-Chem_NO	WRF-Chem_ARI	WRF-Chem_BOTH	WRF-CHIMERE_NO	WRF-CHIMERE_ARI	WRF-CHIMERE_BOTH
Surface shortwave radiation (*172.74* W m^{-2})	Mean_sim	*197.15*	*180.94*	*203.48*	*194.52*	*201.45*	*197.39*	*191.34*	*195.58*
	R	0.76	0.75	0.73	**0.78**	0.75	0.61	0.64	0.66
	MB	24.41	8.21	30.74	21.78	28.71	24.75	18.71	22.94
	NMB (%)	14.13	**4.75**	17.79	12.61	16.62	14.34	10.84	13.29
	NGE (%)	*15.13*	***8.66***	*18.61*	*13.53*	*17.38*	*17.44*	*14.42*	*15.83*
	RMSE	30.25	**20.37**	35.34	26.88	32.80	34.70	29.60	31.45
Surface longwave radiation (*322.3* W m^{-2})	Mean_sim	*316.25*	*315.83*	*312.96*	*312.60*	*312.32*	*313.33*	*314.60*	*314.47*
	R	0.98	0.98	0.98	0.98	0.98	**0.99**	**0.99**	**0.99**
	MB	-6.05	-6.46	-9.34	-9.70	-9.97	-9.66	-8.39	-8.53
	NMB (%)	**-1.88**	-2.00	-2.90	-3.01	-3.09	-2.99	-2.60	-2.64
	NGE (%)	***3.22***	*3.46*	*3.70*	*3.77*	*3.84*	*3.96*	*3.60*	*3.66*
	RMSE	**13.65**	14.13	14.81	14.97	15.17	15.47	14.52	14.72
TOA shortwave radiation (*111.56* W m^{-2})	Mean_sim	*107.76*	*112.68*	*110.38*	*110.95*	*107.16*	*114.33*	*116.62*	*113.09*
	R	**0.81**	0.79	0.69	0.68	0.62	0.65	0.65	0.65
	MB	-3.80	1.13	-1.18	-0.61	-4.40	3.12	5.42	1.89
	NMB (%)	-3.40	**1.01**	-1.05	-0.55	-3.94	2.81	4.87	1.70
	NGE (%)	***10.19***	*10.45*	*11.52*	*10.96*	*11.69*	*14.43*	*14.36*	*12.93*
	RMSE	**15.75**	16.04	17.07	16.10	17.21	20.85	20.67	18.96
TOA longwave radiation (*233.68* W m^{-2})	Mean_sim	*231.54*	*232.26*	*234.34*	*233.96*	*234.39*	*232.52*	*232.17*	*233.18*
	R	0.88	0.90	0.91	0.91	**0.92**	0.74	0.74	0.76
	MB	-2.14	-1.42	0.66	0.28	0.71	-0.61	-0.96	0.05
	NMB (%)	-0.92	-0.61	0.28	**0.12**	0.30	-0.26	-0.41	0.02
	NGE (%)	*2.28*	*2.04*	*1.79*	*1.79*	***1.74***	*3.02*	*2.98*	*2.92*
	RMSE	6.94	6.20	6.00	5.94	**5.86**	10.10	10.07	9.70
Precipitation (*948.91* mm y^{-1})	Mean_sim	*872.42*	*896.98*	*1069.06*	*1056.95*	*1081.84*	*1165.06*	*1160.35*	*1163.77*
	R	**0.71**	**0.71**	**0.71**	**0.71**	0.70	0.69	0.69	0.69
	MB	-76.49	-51.93	120.15	108.04	132.94	207.05	202.35	205.76
	NMB (%)	-9.23	**-8.40**	12.66	11.39	14.01	21.61	21.12	21.48
	NGE (%)	***32.46***	*34.36*	*44.54*	*43.38*	*45.13*	*42.54*	*42.52*	*42.58*
	RMSE	**573.14**	595.76	675.91	668.92	693.74	776.60	786.36	790.73
Cloud cover (*64.09* %)	Mean_sim	*52.51*	*53.32*	*48.18*	*47.80*	*47.46*	*58.12*	*57.98*	*58.55*
	R	0.68	0.68	**0.69**	**0.69**	0.68	0.66	0.66	0.64

	MB	-11.58	-10.77	-16.12	-16.50	-16.83	-6.60	-6.74	-6.18
	NMB (%)	-18.07	-16.80	-25.07	-25.66	-26.18	-10.20	-10.41	**-9.54**
	NGE (%)	*19.48*	*18.87*	*26.01*	*26.56*	*26.97*	*16.74*	*16.92*	***16.72***
	RMSE	16.47	16.28	20.17	20.48	20.73	15.28	15.33	15.34
liquid water path (*88.44* g m^{-2})	Mean_sim	*53.50*	*57.15*	*32.29*	*31.87*	*31.08*	*56.23*	*56.21*	*54.00*
	R	**0.61**	0.58	0.47	0.46	0.28	0.55	0.55	0.51
	MB	-34.94	-31.29	-56.16	-56.58	-57.36	-32.37	-32.40	-34.61
	NMB (%)	-39.51	**-35.38**	-63.49	-63.97	-64.86	-36.54	-36.56	-39.06
	NGE (%)	*57.05*	*57.99*	*66.88*	*67.25*	*67.91*	***53.15***	*53.33*	*56.88*
	RMSE	54.35	54.31	63.54	63.92	67.21	**53.39**	53.42	55.86

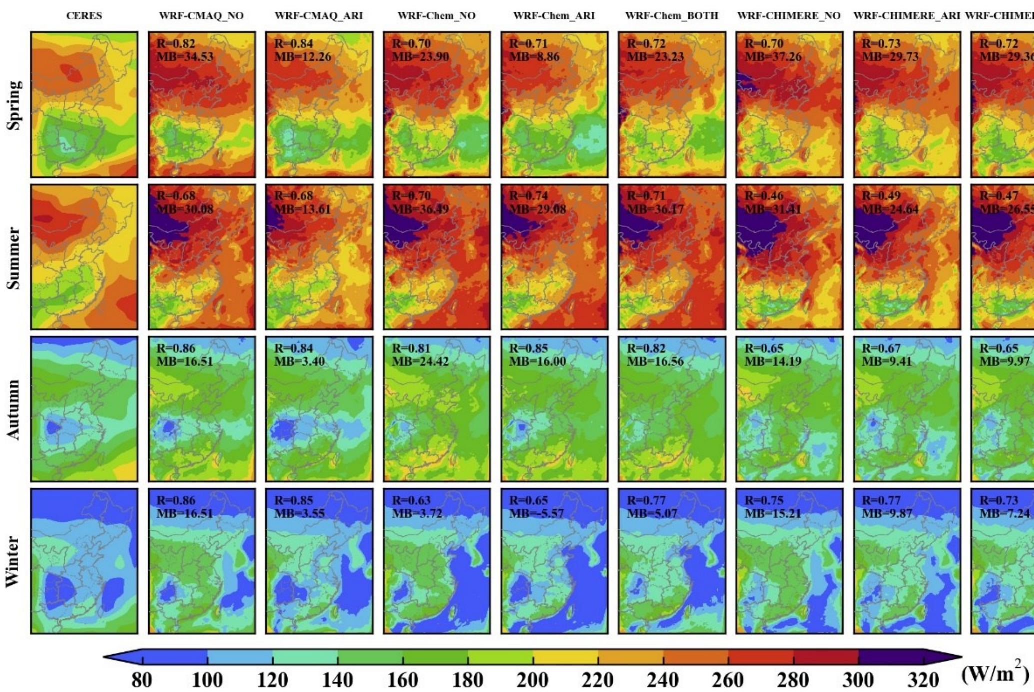

Figure 5. Spatial distributions of seasonal SSR between CERES observations and simulations from WRF-CMAQ, WRF-Chem, and WRF-CHIMERE with and without aerosol feedbacks in eastern China.

4 Multi-model air quality evaluations

In a similar way to meteorology, to further determine the quantitative effects of enabling aerosol feedbacks on the simulation accuracy of air quality variables in eastern China, ground-based and satellite-borne observations were adopted as comparisons in the following evaluation analysis. The usage status of computing resources during each simulation process is also assessed in Section 4.3.

4.1 Ground-based observations

Table 4 and Fig. 7 present the statistical metrics of annual and seasonal air pollutant concentrations ($PM_{2.5}$, O_3, NO_2, SO_2, and CO) simulated by each of the three coupled models. *The evaluations between surface measurements and simulations of $PM_{2.5}$ and O_3 are presented below, and the performance assessments of other gaseous pollutants are in Section 2 of Supplement.*

The R values of annual $PM_{2.5}$ concentrations for WRF-CMAQ (0.68) were the highest, followed by WRF-Chem (0.65–0.68), and WRF-CHIMERE (0.52–0.53). All three models showed higher correlations in winter compared with those in other seasons (Fig. 7). *As shown in Table 4 and Figs. 6–7, WRF-CMAQ underestimated annual and seasonal (except for autumn) $PM_{2.5}$ concentrations with NMBs ranging from −9.78% to −6.39% and −17.68% to +5.17%, respectively. WRF-Chem generated both overestimations and underestimations of $PM_{2.5}$ at the annual and seasonal scales, with related NMBs varying from −39.11% to +24.72%, respectively*. Meanwhile, WRF-CHIMERE excessively overestimated annual and seasonal $PM_{2.5}$ concentrations (NMB: +19.51% to +75.47%). *These biases could be related to different aerosol and gas phase mechanisms, dust and sea salt emission schemes, chemical ICs and BCs, and aerosol size distribution treatments applied in the three two-way coupled models.* Based on the differences in NMBs between simulations with ARI and those with no aerosol feedbacks, ARI-induced annual and seasonal NMB variations of WRF-CMAQ_ARI and WRF-Chem_ARI ranged from +3.01% to +4.21% and +3.07% to +5.02%, respectively, indicating that the enabling of ARI feedbacks slightly reduced annual and seasonal (except for autumn) underestimations of $PM_{2.5}$ concentrations. Note that WRF-CHIMERE_ARI further overestimated the annual and seasonal $PM_{2.5}$, with an increase in NMB of up to 10.04%. The increases in $PM_{2.5}$ concentrations caused by ARI effects can be attributed to synergetic decreases in SSR, T2, WS10, and PBLH, and increases in RH2. With ACI feedbacks further enabled, WRF-Chem_BOTH largely underestimated the annual and seasonal $PM_{2.5}$, with NMBs varying from −24.15% to −14.44% compared with WRF-Chem_ARI. WRF-CHIMERE_BOTH tended to decrease (−2.1% to −0.51%) annual and autumn–winter NMBs, and increase (+0.35% to +3.04%) spring–summer NMBs. Further comparison between ARI- and ACI-induced NMB variations demonstrates the key point that ARI-induced variations in $PM_{2.5}$ concentrations were smaller than those induced by ACI in WRF-Chem, but this pattern was reversed in WRF-CHIMERE. This may be explained by WRF-CHIMERE incorporating the process of dust aerosols serving as IN, which was not included in WRF-Chem in this study.

For O_3, WRF-CHIMERE (R = 0.62) exhibited the highest correlation, followed by WRF-CMAQ (R = 0.55), and WRF-Chem (R = 0.45) (Table 4 and Fig. S16). WRF-CMAQ slightly underestimated annual O_3, with NMBs and NGEs of −12.57% to −11.52%, but WRF-Chem and WRF-CHIMERE both significantly overestimated it, with NMBs of 47.82%–48.10% and 29.46%–29.75%, respectively. The seasonal results of statistical metrics showed patterns that were consistent with annual simulations, and summer O_3 pollution levels were better simulated than those in other seasons (Fig. 6). *All models with ARI feedbacks enabled resulted in slight decreases in annual and seasonal O_3 NMBs and NGEs, ranging from −3.02% to +0.85% (the only positive value of +0.85% was produced by WRF-CMAQ in summer) and from −1.42% to −0.75%, respectively. Meanwhile, for ACI effects, WRF-Chem and WRF-CHIMERE had* *increased annual O_3 NMBs and NGEs of 0.12%−0.65% and 0.40%−0.55%, respectively.* ACI-induced seasonal NMB variations were different for WRF-Chem compared with WRF-CHIMERE; WRF-Chem increased in spring–summer and decreased in autumn–winter, while WRF-CHIMERE increased in all seasons except for winter (Fig. 7). *Such diversity in NMB and NGE variations can be explained by two aspect differences. For model-top boundary conditions, the WRF-CMAQ and WRF-Chem models employed the parameterization scheme of O_3-potential vorticity and WRF-CHIMERE used the climatological data from LMDz-INCA. For gas-phase chemistry mechanisms, three coupled models incorporate a variety of photolytic reactions, with a more comprehensive explanation provided in Section 4.2.*

A comprehensive assessment of the effects of seven gas-phase chemical mechanisms (RADM2, RADMKA, RACM-ESRL, CB05Clx, CB05-TUCL, CBMZ, and MOZART-4) on O_3 simulations via three two-way coupled models (WRF-Chem, WRF-CMAQ, and COSMO-ART) was conducted by Knote et al. (2015); they concluded that the O_3 concentrations simulated via WRF-Chem with the CBMZ mechanism were closest to the mean values of multiple models over North America and Europe in spring and summer. However, in contrast to North America and Europe, the two-way coupled WRF-Chem with CBMZ had the poorest performance during spring in eastern China. In addition, ARI and/or ACI effects contribute to atmospheric dynamics and stability (as mentioned in the PBLH evaluation part of Section 1.1 in Supplment), as well as photochemistry and heterogeneous reactions, and, in turn, they will eventually influence O_3 formation (Xing et al., 2017; Qu et al., 2021; Zhu et al., 2021).

Table 4. Statistical metrics (R, MB, NMB, NGE, and RMSE) between annual simulations and observations of surface $PM_{2.5}$, O_3, NO_2, SO_2, and CO in eastern China. The best results are in bold, while mean simulations and observations are in italics.

Variables	Statistics	WRF-CMAQ_NO	WRF-CMAQ_ARI	WRF-Chem_NO	WRF-Chem_ARI	WRF-Chem_BOTH	WRF-CHIMERE_NO	WRF-CHIMERE_ARI	WRF-CHIMERE_BOTH
$PM_{2.5}$ (*44.99* μg/m^3)	Mean_sim	*40.59*	*42.12*	*44.45*	*46.65*	*38.33*	*62.17*	*65.36*	*65.13*
	R	**0.68**	**0.68**	0.65	0.65	0.69	0.52	0.53	0.53
	MB	-4.40	-2.87	-0.54	1.66	-6.66	17.18	20.37	20.14
	NMB (%)	-9.78	-6.39	**-1.21**	3.69	-14.81	38.19	45.27	44.76
	NGE (%)	***46.41***	*47.08*	*57.82*	*59.91*	*52.10*	*89.85*	*94.10*	*94.01*
	RMSE	**27.62**	27.69	32.58	34.64	32.48	55.13	60.25	59.41
O_3 (*62.23* μg/m^3)	Mean_sim	*55.06*	*54.41*	*88.53*	*87.81*	*87.89*	*76.92*	*76.48*	*76.89*
	R	0.54	0.55	0.46	0.45	0.45	**0.62**	**0.62**	**0.62**
	MB	-7.17	-7.83	26.30	25.58	25.65	14.69	14.25	14.66
	NMB (%)	**-11.52**	-12.57	42.26	41.10	41.22	23.60	22.90	23.55
	NGE (%)	***41.02***	*41.40*	*87.02*	*86.17*	*86.57*	*58.17*	*57.63*	*58.18*
	RMSE	**28.32**	28.68	48.10	47.99	47.82	29.65	29.46	29.75
NO_2 (*31.2* μg/m^3)	Mean_sim	*33.94*	*34.46*	*21.17*	*21.98*	*21.40*	*21.85*	*22.20*	*22.24*
	R	0.59	**0.60**	0.50	0.50	0.50	0.55	0.56	0.56
	MB	2.74	3.26	-10.03	-9.22	-9.80	-9.35	-9.00	-8.96
	NMB (%)	**8.77**	10.44	-32.14	-29.55	-31.40	-29.96	-28.84	-28.73

	NGE (%)	*55.04*	*55.74*	*54.57*	*54.37*	*54.43*	*50.56*	***50.82***	*50.89*
	RMSE	**19.14**	19.48	21.23	21.21	21.21	18.72	18.68	18.70
SO_2 (*18.51* µg/m^3)	Mean_sim	*14.02*	*14.39*	*8.22*	*8.56*	*7.85*	*8.88*	*9.18*	*9.19*
	R	0.40	0.40	0.44	0.44	**0.46**	0.40	0.41	0.41
	MB	-4.49	-4.12	-10.29	-9.95	-10.66	-9.63	-9.33	-9.32
	NMB (%)	-24.25	**-22.24**	-55.61	-53.76	-57.57	-52.02	-50.39	-50.34
	NGE (%)	*75.44*	*76.26*	*64.18*	*64.20*	***66.09***	*75.54*	*75.86*	*75.87*
	RMSE	21.11	21.30	20.13	**20.02**	20.20	22.07	22.17	22.18
CO (*0.96* mg/m^3)	Mean_sim	*0.44*	*0.45*	*0.53*	*0.54*	*0.53*	*0.56*	*0.58*	*0.57*
	R	0.23	0.24	0.21	0.22	0.22	0.47	**0.48**	0.47
	MB	-0.52	-0.51	-0.43	-0.42	-0.43	-0.40	-0.39	-0.39
	NMB (%)	-53.97	-52.99	-45.10	-43.94	-44.68	-41.82	**-40.11**	-40.28
	NGE (%)	*65.44*	*65.11*	*53.63*	*53.38*	*53.80*	*47.27*	***47.08***	*47.09*
	RMSE	0.90	0.90	0.82	0.83	0.83	**0.62**	**0.62**	**0.62**

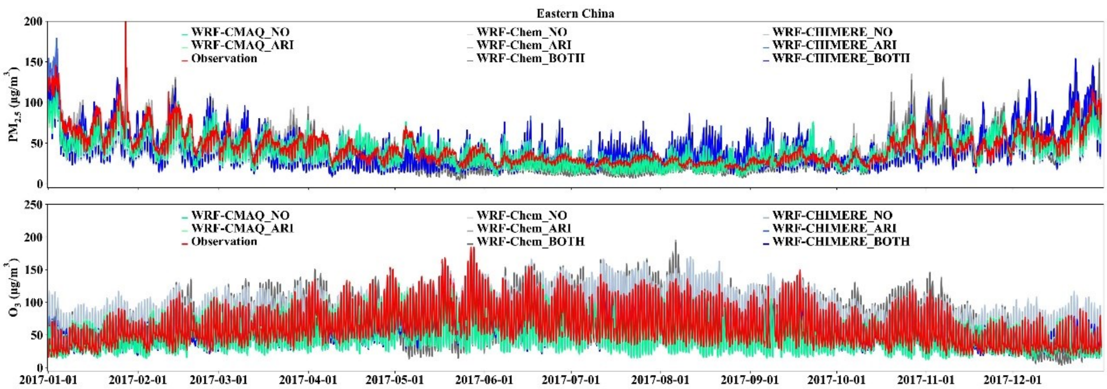

Figure 6. Time series of observed and simulated hourly $PM_{2.5}$ and O_3 concentrations by WRF-CMAQ, WRF-Chem and WRF-CHIMERE with/without aerosol feedbacks over Eastern China during the year of 2017.

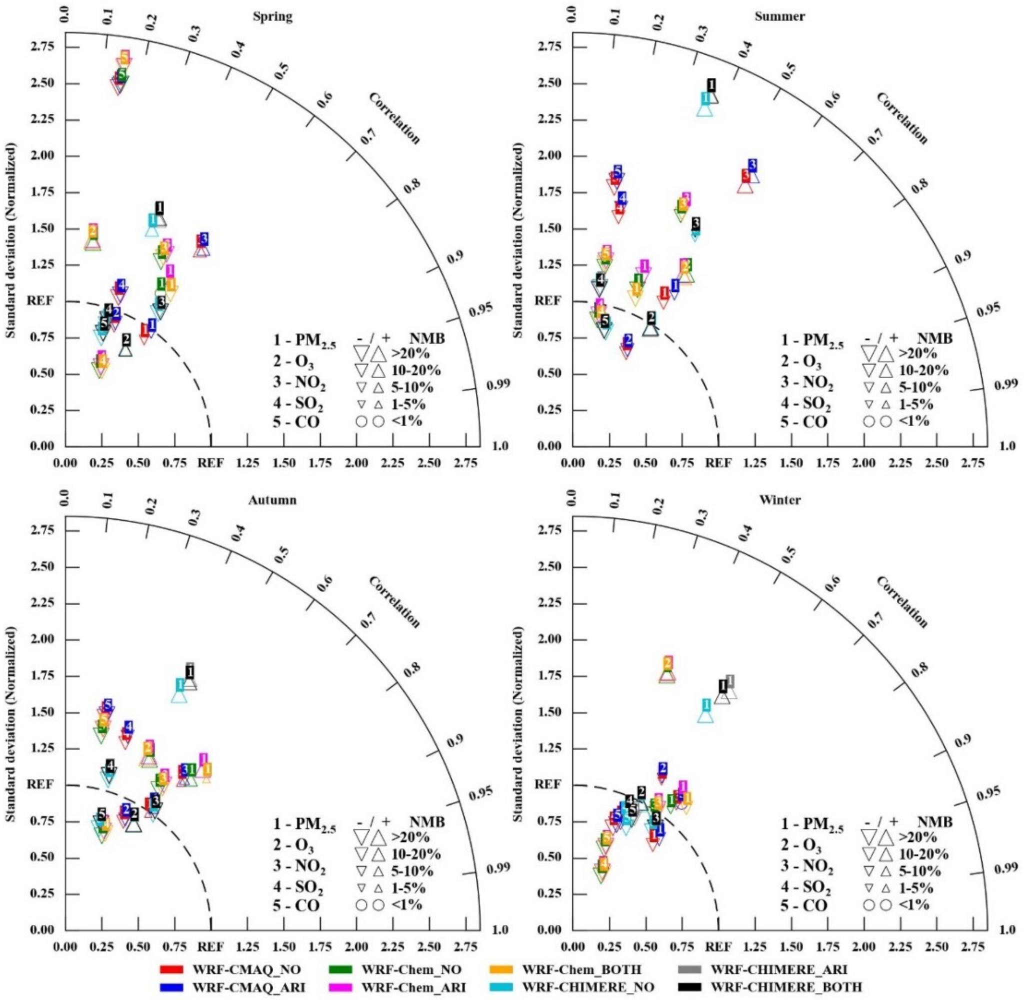

Figure 7. Taylor diagrams (R, normalized standard deviation, and NMB) of seasonal $PM_{2.5}$, O_3, NO_2, SO_2, and CO via three two-way coupled models (WRF-CMAQ, WRF-Chem, and WRF-CHIMERE) with/without ARI and/or ACI effects in eastern China compared with surface observations.

In a similar manner to the meteorological variables presented above, we aimed to conduct quality assurance for the statistical metrics by making further comparisons with $PM_{2.5}$ and O_3 results from previous model evaluations (summarized in Fig. S20). The performances of WRF-CMAQ and WRF-Chem in simulating $PM_{2.5}$ in this study were better than the average levels of previous studies from eastern China. For O_3, WRF-Chem simulations performed worse than the average level of previous studies. Although the R values of O_3 simulated by WRF-CMAQ in this study were lower than the average level of previous studies, the RMSEs in this study were smaller.

4.2 Satellite-borne observations

In this section, we further investigate the discrepancies among different models in terms of the calculated AOD and column concentrations of gases (O_3, NO_2, SO_2, CO, and NH_3), and compare them with various satellite observations. For NH_3, owing to not setting the output of simulated NH_3 concentrations in WRF-CHIMERE, the discussion here only includes the results from WRF-CMAQ and WRF-Chem.

As shown in Table 5, annual AOD at 550 nm, TCO, NO_2, and CO simulated by all three models agreed most closely with satellite observations, with correlation coefficients of 0.80–0.98; these were followed by NH_3 (0.75–0.76), and SO_2 (0.50–0.53). WRF-CMAQ presented negative biases for annual AOD (−0.01), TCO (−5.92 Dobson Units (DU)), SO_2 (−0.03 to −0.02 DU), CO (−1.25 × 10^{17} molecules cm^{-2}), and NH_3 (−2.95 × 10^{15} molecules cm^{-2}), but a positive bias for NO_2 (1.09–1.21 petamolecules cm^{-2}). For AOD, WRF-Chem and WRF-CHIMERE produced positive and negative MBs of +0.09 and −0.06, respectively. Both WRF-Chem and WRF-CHIMERE overestimated NO_2 (0.28–0.63 petamolecules cm^{-2}) and CO (0.93–1.21 × 10^{17} molecules cm^{-2}), and underestimated O_3 (-10.99 to -3.63 DU) and SO_2 (-0.03 to -0.02 DU). Similar to WRF-CMAQ, WRF-Chem also underestimated NH_3 by approximately −3.14 × 10^{15} molecules cm^{-2}.

For seasonal variations, relatively high correlation relationships (0.71–0.88) of AOD were present in autumn, with lower values (0.53–0.84) in other seasons (Fig. 8). WRF-CMAQ and WRF-Chem tended to underestimate AOD in summer (MBs of −0.1 to −0.4) and overestimate it in other seasons (MBs of 0.01–0.05). WRF-CHIMERE had positive biases (0.03–0.04) in winter and negative biases (−0.10 to −0.01) in other seasons. For TCO (Fig. S24), the model performances of WRF-CMAQ and WRF-Chem in spring and winter were slightly better than those in summer and autumn, but all seasonal R values were greater than 0.89. Both WRF-CMAQ (−9.53 to −0.72 DU) and WRF-Chem (−24.62 to +10.57 DU) had negative biases in all seasons (note: WRF-Chem except for autumn). WRF-CHIMERE was better at capturing TCO in spring and summer (overestimations of +9.19 to +29.20 DU) than in autumn and winter (underestimations of −33.75 to −19.40 DU). The R values of NO_2 columns for all three models were slightly higher in autumn and winter (0.82–0.91) than in spring and summer (0.76–0.84). *The seasonal NO_2 columns were generally underestimated in WRF-CMAQ (-0.68 to -0.16 DU), WRF-Chem (-1.40 to -0.44 DU), WRF-CHIMERE (-1.31 to -0.19 DU) (Fig. S22).* All models overestimated SO_2 column concentrations in winter (by approximately 0.01–0.03 DU) but underestimated them in other seasons (−0.05 to −0.001 DU) (Fig. S23). For NH_3, the only primary alkaline gas in the atmosphere, better model performances of WRF-CMAQ and WRF-Chem occurred in summer (R: 0.81–0.87; MB: −3.42 to 2.07 × 10^{15} molecules cm^{-2}) (Fig. S25). Ammonia emissions from fertilizer and livestock have been substantially underestimated in China (Zhang et al., 2017), and peak values occur in spring and summer (Huang et al., 2012). In addition, bidirectional exchanges of fertilizer-induced NH_3 were not considered in our simulations. Compared to above column variables, WRF-CMAQ, WRF-Chem, and WRF-CHIMERE showed relatively poor performances (R: 0.68–0.79) in simulating CO columns during spring, summer, and autumn, respectively, compared with other seasons (Fig. S24). WRF-CMAQ and WRF-CHIMERE respectively underestimated and overestimated CO columns in other seasons except for summer and spring, with MBs of −3.29 to 0.31 × 10^{17} and −0.62 to 2.09 × 10^{17} molecules cm^{-2}, respectively. WRF-Chem had positive MBs in summer and autumn (4.03–5.12 × 10^{17} molecules cm^{-2}) and negative MBs in spring and winter (−3.15 to −2.10 × 10^{17} molecules cm^{-2}).

Moreover, after comparing the performance results for each pollutant between sections 4.1 and 4.2, the only disparity found between evaluations with ground-based observations compared with those with satellite-borne observations was for CO. The formation of CO via the oxidation of methane, an important source of CO emissions (Stein et al., 2014), is not considered in the three coupled models, and methane emissions are not included in the MEIC inventory. In addition, the contribution of CO to atmospheric oxidation capacity (OH radicals) was non-negligible (e.g., values were approximately 20.54%–38.97% in Beijing (Liu et al., 2021), and 26%–31% in Shanghai (Zhu et al., 2020). Also, these discrepancies in the model performances for simulating AOD and column concentrations of gases can be explained by differences in the representations of aerosol species groups, Fast-JX photolysis scheme, and gas-phase mechanisms in the three coupled models. *More detailed interpretations were grouped into four aspects: (1) AODs are calculated via Mie theory using refractive indices of different numbers (5, 6 and 10) of aerosol species group in different coupled models (WRF-CMAQ, WRF-Chem and WRF-CHIMERE) (Tables S5–S6); (2) 7 (294.6, 303.2, 310.0, 316.4, 333.1, 382.0 and 607.7 nm), 4 (300, 400, 600 and 999 nm), and 5 (200, 300, 400, 600, and 999 nm) effective wavelengths are used in calculating actinic fluxes and photolysis rates in Fast-JX photolysis modules of WRF-CMAQ, WRF-Chem and WRF-CHIMERE, respectively;(3) Different calculating methods of aerosol and cloud optical properties exist in the Fast-JX schemes of three coupled models (Tables S1 and S5–S6); (4) 77, 52 and 40 gas-phase species involve 218, 132, 120 gas-phase reactions in CB6, CBMZ and MELCHIOR2 mechanisms, respectively.*

When all three models enabled just ARI effects, improvements in annual AOD and NO_2 columns simulated by these models were relatively limited. The AOD simulations improved in spring and summer, but worsened in autumn and winter (Table 4 and Fig. 9). Larger variations in seasonal MBs of NO_2 columns induced by ARI effects occurred in WRF-CMAQ (−0.18 to 0.13 petamolecules cm^{-2}) compared with WRF-Chem and WRF-CHIMERE (0–0.01 petamolecules cm^{-2}). When both ARI and ACI effects were enabled in WRF-Chem, the model performance for seasonal AOD simulations worsened considerably. The annual and seasonal NO_2 simulations via WRF-Chem became slightly worse, while those using WRF-CHIMERE became slightly better. In contrast to AOD and NO_2 column concentrations, improvements in annual and seasonal column simulations of total ozone, PBL SO_2, and NH_3 via all two-way coupled models were limited when one or both of ARI and ACI were enabled.

Table 5. Statistical metrics (R, MB, NMB, *NGE*, and RMSE) of simulated and satellite-retrieved AOD, total column ozone, tropospheric column NO_2, PBL column SO_2, total column CO, and total column density of NH_3 in eastern China. The best results are in bold, while annual mean simulations and observations are in italics.

Variables	Statistics	WRF-CMAQ_NO	WRF-CMAQ_ARI	WRF-Chem_NO	WRF-Chem_ARI	WRF-Chem_BOTH	WRF-CHIMERE_NO	WRF-CHIMERE_ARI	WRF-CHIMERE_BOTH
AOD (*0.27*)	Mean_sim	*0.26*	*0.27*	*0.35*	*0.36*	*0.25*	*0.21*	*0.22*	*0.22*
	R	0.80	0.80	0.80	0.80	0.75	**0.87**	**0.87**	0.86
	MB	-0.01	-0.01	0.09	0.09	-0.01	-0.05	-0.05	-0.04
	NMB (%)	-3.99	**-2.93**	34.14	35.03	-4.92	-18.72	-17.37	-16.22
	NGE (%)	*34.90*	*34.82*	*58.21*	*58.89*	*41.46*	*32.15*	***32.11***	*32.06*
	RMSE	**0.09**	**0.09**	0.15	0.15	0.10	**0.09**	**0.09**	0.10

O_3 VCDs (*312.07* DU)	Mean_sim	*306.15*	*306.15*	*300.77*	*300.73*	*300.46*	*307.69*	*307.47*	*307.75*
	R	**0.98**	**0.98**	0.97	0.97	0.97	0.65	0.65	0.65
	MB	-5.92	-5.92	-10.68	-10.72	-10.99	-3.69	-3.91	-3.63
	NMB (%)	-1.90	-1.90	-3.43	-3.44	-3.53	-1.19	-1.26	**-1.17**
	NGE (%)	***2.46***	***2.46***	*25.02*	*25.02*	*25.08*	*10.95*	*10.89*	*10.93*
	RMSE	**8.91**	**8.91**	83.72	83.73	83.94	39.88	39.71	39.73
Tropospheric NO_2 VCDs (*2.71×10^15^* molecules cm^{-2})	Mean_sim	*3.80*	*3.91*	*3.07*	*3.08*	*3.06*	*2.62*	*2.63*	*2.63*
	R	0.85	0.85	**0.87**	**0.87**	**0.87**	**0.87**	**0.87**	**0.87**
	MB	1.09	1.21	0.62	0.63	0.61	0.28	0.29	0.29
	NMB (%)	40.35	44.64	25.27	25.52	24.89	**12.03**	12.47	12.42
	NGE (%)	*52.80*	*55.08*	*46.01*	*46.05*	***45.17***	*46.06*	*46.31*	*46.24*
	RMSE	3.18	3.33	2.27	2.27	2.27	**1.65**	1.67	1.68
PBL SO_2 VCDs (*0.09* DU)	Mean_sim	*0.07*	*0.07*	*0.09*	*0.09*	*0.06*	*0.06*	*0.06*	*0.06*
	R	0.53	0.53	**0.56**	**0.56**	0.54	0.50	0.50	0.50
	MB	-0.03	-0.02	-0.03	-0.02	-0.03	-0.03	-0.02	-0.02
	NMB (%)	-27.32	-25.48	-32.50	**-21.50**	-35.08	-28.64	-27.31	-27.51
	NGE (%)	***57.45***	*58.26*	*67.55*	*68.07*	*64.83*	*68.31*	*68.61*	*68.80*
	RMSE	**0.07**	**0.07**	0.08	0.08	**0.07**	**0.07**	**0.07**	**0.07**
Total CO VCDs (*21.60×10^17^* molecules cm^{-2})	Mean_sim	*20.34*	*20.35*	*22.20*	*22.20*	*22.21*	*22.34*	*22.36*	*22.35*
	R	0.83	0.83	**0.87**	**0.87**	**0.87**	0.86	0.86	0.86
	MB	-1.26	-1.24	0.93	0.93	0.94	1.19	1.21	1.19
	NMB (%)	-5.83	-5.75	**4.35**	4.37	4.44	5.64	5.70	5.65
	NGE (%)	*9.33*	***9.31***	*10.30*	*10.28*	*10.32*	*11.02*	*11.06*	*11.10*
	RMSE	**2.54**	**2.54**	2.69	2.68	2.69	2.57	2.58	2.58
Total NH_3 VCDs (*16.05×10^15^* molecules cm^{-2})	Mean_sim	*13.06*	*13.15*	*12.31*	*12.27*	*8.63*	NA	NA	NA
	R	**0.76**	**0.76**	0.73	0.73	0.76	NA	NA	NA
	MB	-3.00	-2.90	-3.27	-3.32	-3.34	NA	NA	NA
	NMB (%)	-18.66	**-18.08**	-21.01	-21.28	-21.41	NA	NA	NA
	NGE (%)	***47.69***	*48.09*	*50.84*	*50.80*	*50.99*	*NA*	*NA*	*NA*
	RMSE	**9.26**	9.47	9.48	9.46	9.61	NA	NA	NA

NA indicates that outputs of NH_3 column concentrations were not extracted from WRF-CHIMERE with/without aerosol feedback simulations.

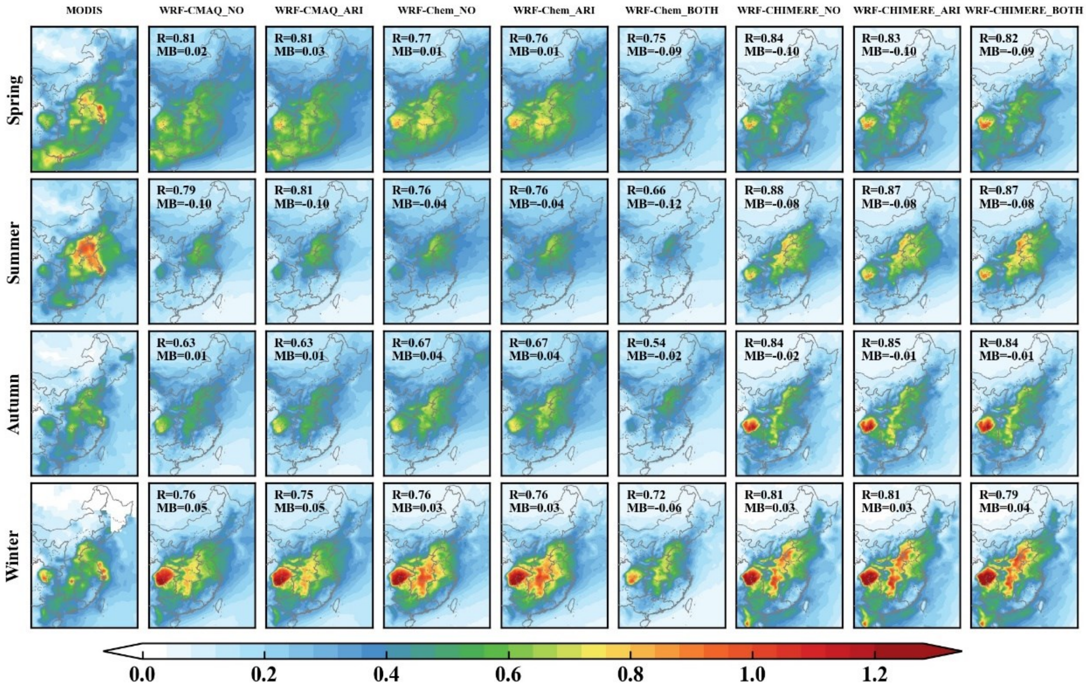

Figure 8. Spatial distributions of seasonal AOD between MODIS observations and simulations from WRF-CMAQ, WRF-Chem, and WRF-CHIMERE with and without aerosol feedbacks in eastern China.

4.3 Computational performance

Table 5 summarizes the comparative results of central processing unit (CPU) time consumption for one day simulations via WRF-CMAQ, WRF-Chem, and WRF-CHIMERE with and without aerosol feedbacks in 2017. The results show that regardless of whether aerosol feedbacks were enabled, the CPU time consumed by WRF-CMAQ simulating one-day meteorology and air quality was shortest, followed by WRF-CHIMERE, and WRF-Chem. Compared with simulations without aerosol feedbacks, the processing time of WRF-CMAQ with ARI enabled increased by 0.22–0.34 hours per day, while increases in the running time of WRF-Chem and WRF-CHIMERE were not significant (0.02–0.03 hours per day). The CPU time for both WRF-Chem and WRF-CHIMERE with both ARI and ACI effects enabled was slightly increased, and the increase in CPU time for the former (0.25 hours per day) was larger than that for the latter (0.11 hours per day). Compared with WRF-CMAQ and WRF-Chem, the CPU time of WRF-CHIMERE showed obvious seasonal differences, with the time in winter and spring being significantly longer than that in summer and autumn. These differences can be partially explained by the choice of main configurations, including model resolution, model version, and parametrization schemes (cloud microphysics, PBL, cumulus, surface layer, land surface, gas-phase chemistry, and aerosol mechanisms).

Table 5. Summary of running time for different coupled models.

Month	WRF-CMAQ (hour)		WRF-Chem (hour)			WRF-CHIMERE (hour)		
	NO	ARI	NO	ARI	BOTH	NO	ARI	BOTH
Jan.	0.37	0.59	0.69	0.71	0.96	0.67	0.70	0.77
Feb.	0.35	0.60	0.68	0.70	0.93	0.64	0.67	0.73
Mar.	0.39	0.65	0.70	0.72	1.00	0.59	0.62	0.72
Apr.	0.37	0.67	0.67	0.69	0.92	0.54	0.57	0.65
May	0.39	0.71	0.61	0.66	0.86	0.52	0.55	0.62
June	0.40	0.74	0.66	0.67	0.95	0.48	0.51	0.63
July	0.36	0.69	0.65	0.67	0.86	0.49	0.50	0.58
Aug.	0.38	0.68	0.66	0.68	0.90	0.49	0.52	0.61
Sept.	0.37	0.63	0.64	0.65	0.89	0.48	0.52	0.63
Oct.	0.38	0.62	0.66	0.68	0.94	0.53	0.56	0.69
Nov.	0.36	0.58	0.68	0.70	0.91	0.64	0.67	0.72
Dec.	0.35	0.57	0.63	0.66	0.87	0.67	0.70	0.74

5 Conclusions

Applications of two-way coupled meteorology and air quality models have been performed in eastern China in recent years, but no research focused on the comprehensive assessments of multiple coupled models in this region. To the best of our knowledge, this is the first time to conduct comprehensive inter-comparisons among the open-sourced two-way coupled meteorology and air quality models (WRF-CMAQ, WRF-Chem, and WRF-CHIMERE). This study systemically evaluated the hindcast simulations for 2017 and explored the impacts of ARI and/or ACI on model and computational performances in eastern China.

After detailed comparisons with ground-based and satellite-borne observations, the evaluation results showed that three coupled models perform well for meteorology and air quality, especially for surface temperature (with R up to 0.97) and $PM_{2.5}$ concentrations (with R up to 0.68). The effects of aerosol feedbacks on model performances varied depending on the two-way coupled models, variables, and time scales. There were around 20%–70% increase of computational time when these two-way coupled models enabled aerosol feedbacks against simulations without aerosol-radiation-cloud interactions. It is noteworthy that all three coupled models could well reproduce the spatiotemporal distributions of satellite-retrieved CO column concentrations but not for ground-observed CO concentrations.

With inter-comparisons, some uncertainty sources can be ascertained in evaluating aerosol feedback effects. As numerous schemes can be combined in configurations of different coupled models, here we only evaluated simulations with specific settings. Future comparison works with considering more combinations of multiple schemes within the same or different coupled models need to be conducted. Among the three coupled models, the numerical representations for specific variable in same scheme are diverse, e.g., treatments of cloud cover and cloud optical properties in the Fast-JX photolysis scheme. More accurate representations of photolysis *processes should be taken into account to reduce the evaluation uncertainties. In addition, FDDA nudging technique can attenuate the ARI effects during severe air polluted episodes, and optimal nudging coefficients among different regions need to be determined. Last but not least, the actual mechanisms underlying ACI effects are still unclear, and the new advances in the measurements and parameterizations of CCN/IN activations and precipitation need to be timely incorporated in coupled models.*

Code availability

The source codes of the two-way coupled WRF v4.1.1-CMAQ v5.3.1, WRF-Chem v4.1.1, and WRF v3.7.1-CHIMERE v2020r1 models are obtained from https://github.com/USEPA/CMAQ, https://github.com/wrf-model/WRF, and https://www.lmd.polytechnique.fr/chimere, respectively (last access: November 2020). *The related source codes, configuration information, namelist files and automated run scripts of these three two-way coupled models are archived at Zenodo with the associated DOI: https://doi.org/10.5281/zenodo.7901682 (Gao et al., 2023a; link: https://zenodo.org/record/7901682).*

Data availability

The meteorological ICs and BCs used for three coupled models can be obtained at https://doi.org/10.5281/zenodo.7925012 (Gao et al., 2023b; link: https://zenodo.org/record/7925012). The Chemical ICs and BCs used for WRF-CMAQ, WRF-Chem and WRF-CHIMERE are available at https://doi.org/10.5281/zenodo.7932390 (Gao et al., 2023c; link: https://zenodo.org/record/7932390), https://doi.org/10.5281/zenodo.7932936 (Gao et al., 2023d; link: https://zenodo.org/record/7932936), and https://doi.org/10.5281/zenodo.7933641 (Gao et al., 2023e; link: https://zenodo.org/record/7933641), respectively. The emission data used for WRF-CMAQ, WRF-Chem and WRF-CHIMERE can be downloaded from https://doi.org/10.5281/zenodo.7932430 (Gao et al., 2023f; link: https://zenodo.org/record/7932430), https://doi.org/10.5281/zenodo.7932734 (Gao et al., 2023g; link: https://zenodo.org/record/7932734), and https://doi.org/10.5281/zenodo.7931614 (Gao et al., 2023h; link: https://zenodo.org/record/7931614), respectively. The DOIs and links regarding the output data of each simulation scenario are presented in Table S9. All data used to create figures and tables in this study are provided in an open repository on Zenodo (https://doi.org/10.5281/zenodo.7750907, Gao et al., 2023i; link: https://zenodo.org/record/7750907).

Author contributions

CG, ZX, AX performed the majority of the source code configuration of WRF-CMAQ, WRF-Chem and WRF-CHIMERE, designed the numerical simulations to carry them out, related analysis, figure plotting, and paper writing. QT, HZ, SZ, GY, MZ and XS were involved with the original research plan and made suggestions for the paper writing.

Competing interests

The contact author has declared that neither they nor their co-authors have any competing interests.

Acknowledgements

The authors are very grateful to David Wong, Chun Zhao and Laurent Menut who provided detailed information on the two-way coupled WRF-CMAQ, WRF-Chem and WRF-CHIMERE models, respectively.

Financial support

This study was financially sponsored by the Youth Innovation Promotion Association of Chinese Academy of Sciences, China (grant nos. 2022230), the National Key Research and Development Program of China (grant nos. 2017YFC0212304 & 2019YFE0194500), the Talent Program of Chinese Academy of Sciences (Y8H1021001), and the National Natural Science Foundation of China (grant nos. 42171142 & 41771071).

References

Abdul-Razzak, H. and Ghan, S. J.: A parameterization of aerosol activation 3. Sectional representation, J. Geophys. Res. Atmos., 107, AAC-1, https://doi.org/10.1029/2001JD000483, 2002.

Alapaty, K., Herwehe, J. A., Otte, T. L., Nolte, C. G., Bullock, O. R., Mallard, M. S., Kain, J. S., and Dudhia, J.: Introducing subgrid-scale cloud feedbacks to radiation for regional meteorological and climate modeling, Geophys. Res. Lett., 39, 1–5, https://doi.org/10.1029/2012GL054031, 2012.

Archer-Nicholls, S., Lowe, D., Utembe, S., Allan, J., Zaveri, R. A., Fast, J. D., Hodnebrog, Ø., Denier Van Der Gon, H., and Mcfiggans, G.: Gaseous chemistry and aerosol mechanism developments for version 3.5.1 of the online regional model, WRF-Chem, Geosci. Model Dev., 7, 2557–2579, https://doi.org/10.5194/gmd-7-2557-2014, 2014.

Baklanov, A., Schlünzen, K., Suppan, P., Baldasano, J., Brunner, D., Aksoyoglu, S., Carmichael, G., Douros, J., Flemming, J., and Forkel, R.: Online coupled regional meteorology chemistry models in Europe: current status and prospects, Atmos. Chem. Phys., 14, 317–398, https://doi.org/10.5194/acp-14-317-2014, 2014.

Balzarini Briant, R., Tuccella, P., Deroubaix, A., Khvorostyanov, D., Menut, L., Mailler, S., and Turquety, S.: Aerosol-radiation interaction modelling using online coupling between the WRF 3.7.1 meteorological model and the CHIMERE 2016 chemistry-transport model, through the OASIS3-MCT coupler, Geosci. Model Dev., 10, 927–944, https://doi.org/10.5194/gmd-10-927-2017, 2017.

Briant, R., Tuccella, P., Deroubaix, A., Khvorostyanov, D., Menut, L., Mailler, S., and Turquety, S.: Aerosol-radiation interaction modelling using online coupling between the WRF 3.7.1 *meteorological model and the CHIMERE 2016 chemistry-transport model, through the OASIS3-MCT coupler, Geosci. Model Dev., 10, 927–944, https://doi.org/10.5194/gmd-10-927-2017, 2017.*

Brunner, D., Savage, N., Jorba, O., Eder, B., Giordano, L., Badia, A., Balzarini, A., Baro, R., Bianconi, R., and Chemel, C.: Comparative analysis of meteorological performance of coupled chemistry-meteorology models in the context of AQMEII phase 2, Atmos. Environ., 115, 470–498, https://doi.org/10.1016/j.atmosenv.2014.12.032, 2015.

Campbell, P., Zhang, Y., Wang, K., Leung, R., Fan, J., Zheng, B., Zhang, Q., and He, K.: Evaluation of a multi-scale WRF-CAM5 simulation during the 2010 East Asian Summer Monsoon, Atmos. Environ., 169, 204–217, https://doi.org/10.1016/j.atmosenv.2017.09.008, 2017.

Carslaw, K. S., Boucher, O., Spracklen, D. V, Mann, G. W., Rae, J. G. L., Woodward, S., and Kulmala, M.: A review of natural aerosol interactions and feedbacks within the Earth system, Atmos. Chem. Phys., 10, 1701–1737, https://doi.org/10.5194/acp-10-1701-2010, 2010.

Chapman, E. G., Jr, W. I. G., Easter, R. C., Barnard, J. C., Ghan, S. J., Pekour, M. S., and Fast, J. D.: and Physics Coupling aerosol-cloud-radiative processes in the WRF-Chem model : Investigating the radiative impact of elevated point sources, 945–964, https://doi.org/10.5194/acp-9-945-2009, 2009.

Chen, L., Gao, Y., Zhang, M., Fu, J. S., Zhu, J., Liao, H., Li, J., Huang, K., Ge, B., and Wang, X.: MICS-Asia III: Multi-model comparison and evaluation of aerosol over East Asia, Atmos. Chem. Phys., 19, 11911–11937, https://doi.org/10.5194/acp-19-11911-2019, 2019.

Ding, Q. J., Sun, J., Huang, X., Ding, A., Zou, J., Yang, X., and Fu, C.: Impacts of black carbon on the formation of advection–radiation fog during a haze pollution episode in eastern China, Atmos. Chem. Phys., 19, 7759–7774, https://doi.org/10.5194/acp-19-7759-2019, 2019.

Dionne, J., von Salzen, K., Cole, J., Mahmood, R., Leaitch, W. R., Lesins, G., Folkins, I., and Chang, R. Y.-W.: Modelling the relationship between liquid water content and cloud droplet number concentration observed in low clouds in the summer Arctic and its radiative effects, Atmos. Chem. Phys., 20, 29–43, https://doi.org/10.5194/acp-20-29-2020, 2020.

Fan, J., Wang, Y., Rosenfeld, D., and Liu, X.: Review of aerosol-cloud interactions: Mechanisms, significance, and challenges, J. Atmos. Sci., 73, 4221–4252, https://doi.org/10.1175/JAS-D-16-0037.1, 2016.

Feng, X., Lin, H., Fu, T.-M., Sulprizio, M. P., Zhuang, J., Jacob, D. J., Tian, H., Ma, Y., Zhang, L., and Wang, X.: WRF-GC (v2.0): online two-way coupling of WRF (v3.9.1.1) and GEOS-Chem (v12.7.2) for modeling regional atmospheric chemistry–meteorology interactions, Geosci. Model Dev., 14, 3741–3768, https://doi.org/10.5194/gmd-14-3741-2021, 2021.

Forkel, R., Werhahn, J., Hansen, A. B., McKeen, S., Peckham, S., Grell, G., and Suppan, P.: Effect of aerosol-radiation feedback on regional air quality–A case study with WRF/Chem, Atmos. Environ., 53, 202–211, https://doi.org/10.1016/j.atmosenv.2011.10.009,

Gao, C., Zhang, X., Xiu, A., Huang, L., Zhao, H., Wang, K., and Tong, Q.: Spatiotemporal distribution of biogenic volatile organic compounds emissions in China, Acta Sci. Circumstantiae, 39, 4140–4151, https://doi.org/10.13671/j.hjkxxb.2019.0243, 2019.

Gao, C., Xiu, A., Zhang, X., Tong, Q., Zhao, H., Zhang, S., Yang, G., and Zhang, M.: Two-way coupled meteorology and air quality models in Asia: a systematic review and meta-analysis of impacts of aerosol feedbacks on meteorology and air quality, Atmos. Chem. Phys., 22, 5265–5329, https://doi.org/10.5194/acp-22-5265-2022, 2022.

Gao, C., Xiu, A., Zhang, X.: Oservational data for sfdda nudging analysis in WRF model over China during 2017, Zenodo [Data set], https://doi.org/10.5281/zenodo.6975602, 2022.
Gao, C., Xiu, A., Zhang, X., Tong, Q., Zhao, H., Zhang, S., Yang, G., Zhang, M., Xie, S.: Source codes of WRF v4.1.1-CMAQ v5.3.1, WRF-Chem v4.1.1 and WRF v3.7.1-CHIMERE v2020r1, Zenodo [software]. https://doi.org/10.5281/zenodo.7901682, 2023a.
Gao, C., Xiu, A., Zhang, X., Tong, Q., Zhao, H., Zhang, S., Yang, G., Zhang, M., Xie, S.: FNL data used for producing meteorological ICs/BCs of WRF v4.1.1-CMAQ v5.3.1, WRF-Chem v4.1.1 and WRF v3.7.1-CHIMERE v2020r1, Zenodo [data set], https://doi.org/10.5281/zenodo.7925012, 2023b.
Gao, C., Xiu, A., Zhang, X., Tong, Q., Zhao, H., Zhang, S., Yang, G., Zhang, M., Xie, S.: Chemical initial and boundary conditions for WRF-CMAQ, Zenodo [data set], https://doi.org/10.5281/zenodo.7932390, 2023c.
Gao, C., Xiu, A., Zhang, X., Tong, Q., Zhao, H., Zhang, S., Yang, G., Zhang, M., Xie, S.: Chemical initial and boundary conditions for WRF-Chem. Zenodo [data set], https://doi.org/10.5281/zenodo.7932936, 2023d.
Gao, C., Xiu, A., Zhang, X., Tong, Q., Zhao, H., Zhang, S., Yang, G., Zhang, M., Xie, S.: Chemical initial and boundary conditions for WRF-CHIMERE, Zenodo [data set], https://doi.org/10.5281/zenodo.7933641, 2023e.
Chao Gao, Xuelei Zhang, Aijun Xiu, Qingqing Tong, Hongmei Zhao, Shichun Zhang, Guangyi Yang, Mengduo Zhang, Shengjin Xie: Emission input data for WRF-CMAQ, Zenodo [data set], https://doi.org/10.5281/zenodo.7932430, 2023f.
Gao, C., Xiu, A., Zhang, X., Tong, Q., Zhao, H., Zhang, S., Yang, G., Zhang, M., Xie, S.: Emission input data for WRF-Chem, Zenodo [data set], https://doi.org/10.5281/zenodo.7932734, 2023g.
Gao, C., Xiu, A., Zhang, X., Tong, Q., Zhao, H., Zhang, S., Yang, G., Zhang, M., Xie, S.: Emission input data for WRF-CHMIERE, Zenodo [data set], https://doi.org/10.5281/zenodo.7931614, 2023h.
Gao, C., Xiu, A., Zhang, X., Tong, Q., Zhao, H., Zhang, S., Yang, G., Zhang, M., Xie, S.: Data used to create figures and tables in the GMD manuscript "Inter-comparison of multiple two-way coupled meteorology and air quality models (WRF v4.1.1-CMAQ v5.3.1, WRF-Chem v4.1.1 and WRF v3.7.1-CHIMERE v2020r1) in eastern China", Zenodo [data set], https://doi.org/10.5281/zenodo.7750907, 2023i.
Gao, J., Woodward, A., Vardoulakis, S., Kovats, S., Wilkinson, P., Li, L., Xu, L., Li, J., Yang, J., and Cao, L.: Haze, public health and mitigation measures in China: A review of the current evidence for further policy response, Sci. Total Environ., 578, 148–157, https://doi.org/10.1016/j.scitotenv.2016.10.231, 2017.
Gao, M., Han, Z., Liu, Z., Li, M., Xin, J., Tao, Z., Li, J., Kang, J. E., Huang, K., Dong, X., Zhuang, B., Li, S., Ge, B., Wu, Q., Cheng, Y., Wang, Y., Lee, H. J., Kim, C. H., Fu, J. S., Wang, T., Chin, M., Woo, J. H., Zhang, Q., Wang, Z., and Carmichael, G. R.: Air quality and climate change, Topic 3 of the Model Inter-Comparison Study for Asia Phase III (MICS-Asia III)- Part 1: Overview and model evaluation, Atmos. Chem. Phys., 18, 4859–4884, https://doi.org/10.5194/acp-18-4859-2018, 2018.
Gao, M., Han, Z., Tao, Z., Li, J., Kang, J.-E., Huang, K., Dong, X., Zhuang, B., Li, S., and Ge, B.:

Air quality and climate change, Topic 3 of the Model Inter-Comparison Study for Asia Phase III (MICS-Asia III)–Part 2: aerosol radiative effects and aerosol feedbacks, Atmos. Chem. Phys., 20, 1147–1161, https://doi.org/10.5194/acp-20-1147-2020, 2020.

Gao, Y., Zhang, M., Liu, Z., Wang, L., Wang, P., Xia, X., Tao, M., and Zhu, L.: Modeling the feedback between aerosol and meteorological variables in the atmospheric boundary layer during a severe fog-haze event over the North China Plain., Atmos. Chem. Phys., 15, 4279–4295, https://doi.org/10.5194/acp-15-4279-2015, 2015.

Ge, B., Itahashi, S., Sato, K., Xu, D., Wang, J., Fan, F., Tan, Q., Fu, J. S., Wang, X., and Yamaji, K.: Model Inter-Comparison Study for Asia (MICS-Asia) phase III: multimodel comparison of reactive nitrogen deposition over China, Atmos. Chem. Phys., 20, 10587–10610, https://doi.org/10.5194/acp-20-10587-2020, 2020.

Geng, G., Zheng, Y., Zhang, Q., Xue, T., Zhao, H., Tong, D., Zheng, B., Li, M., Liu, F., and Hong, C.: Drivers of PM2.5 air pollution deaths in China 2002–2017, Nat. Geosci., 14, 645–650, https://doi.org/10.1038/s41561-021-00792-3, 2021.

Gillies, S., Ward, B., and Petersen, A. S.: Rasterio: Geospatial raster I/O for Python programmers, URL https//github.com/mapbox/rasterio, 2013.

Govardhan, G. R., Nanjundiah, R. S., Satheesh, S. K., Moorthy, K. K., and Takemura, T.: Inter-comparison and performance evaluation of chemistry transport models over Indian region, Atmos. Environ., 125, 486–504, https://doi.org/10.1016/j.atmosenv.2015.10.065, 2016.

Grell, G. and Baklanov, A.: Integrated modeling for forecasting weather and air quality: A call for fully coupled approaches, Atmos. Environ., 45, 6845–6851, https://doi.org/10.1016/j.atmosenv.2011.01.017, 2011.

Grell, G. A., Peckham, S. E., Schmitz, R., McKeen, S. A., Frost, G., Skamarock, W. C., and Eder, B.: Fully coupled "online" chemistry within the WRF model, Atmos. Environ., 39, 6957–6975, https://doi.org/10.1016/j.atmosenv.2005.04.027, 2005.

Guo, J., Li, Y., Cohen, J. B., Li, J., Chen, D., Xu, H., Liu, L., Yin, J., Hu, K., and Zhai, P.: Shift in the temporal trend of boundary layer height in China using long-term (1979-2016) radiosonde data, Geophys. Res. Lett., 46, 6080–6089, https://doi.org/10.1029/2019GL082666, 2019.

He, K., Huo, H., and Zhang, Q.: Urban air pollution in China: current status, characteristics, and progress, Annu. Rev. Environ. Resour., 27, 397, https://doi.org/10.1146/annurev.energy.27.122001.083421, 2002.

Hogrefe, C., Bash, J. O., Pleim, J. E., Schwede, D. B., Gilliam, R. C., Foley, K. M., Appel, K. W., and Mathur, R.: An Analysis of CMAQ Gas Phase Dry Deposition over North America Through Grid-Scale and Land-Use Specific Diagnostics in the Context of AQMEII4, Atmos. Chem. Phys. Discuss., 1–52, https://doi.org/10.5194/acp-2023-10, 2023.

Hong, C., Zhang, Q., Zhang, Y., Tang, Y., Tong, D., and He, K.: Multi-year downscaling application of two-way coupled WRF v3.4 and CMAQ v5.0.2 over east Asia for regional climate and air quality modeling: model evaluation and aerosol direct effects., Geosci. Model Dev., 10, 2447–2470, https://doi.org/10.5194/gmd-10-2447-2017, 2017.

Huang, D. and Gao, S.: Impact of different reanalysis data on WRF dynamical downscaling over China, Atmos. Res., 200, 25–35, https://doi.org/10.1016/j.atmosres.2017.09.017, 2018.

Huang, X., Song, Y., Li, M., Li, J., Huo, Q., Cai, X., Zhu, T., Hu, M., and Zhang, H.: A high-resolution ammonia emission inventory in China, Global Biogeochem. Cycles, 26, https://doi.org/10.1029/2011GB004161, 2012.

Iacono, M. J., Delamere, J. S., Mlawer, E. J., Shephard, M. W., Clough, S. A., and Collins, W. D.: Radiative forcing by long‐lived greenhouse gases: Calculations with the AER radiative transfer models, J. Geophys. Res. Atmos., 113, https://doi.org/10.1029/2008JD009944, 2008.

Im, U., Bianconi, R., Solazzo, E., Kioutsioukis, I., Badia, A., Balzarini, A., Baró, R., Bellasio, R., Brunner, D., and Chemel, C.: Evaluation of operational on-line-coupled regional air quality models over Europe and North America in the context of AQMEII phase 2. Part I: Ozone, Atmos. Environ., 115, 404–420, https://doi.org/10.1016/j.atmosenv.2014.09.042, 2015a.

Im, U., Bianconi, R., Solazzo, E., Kioutsioukis, I., Badia, A., Balzarini, A., Baró, R., Bellasio, R., Brunner, D., and Chemel, C.: Evaluation of operational online-coupled regional air quality models over Europe and North America in the context of AQMEII phase 2. Part II: Particulate matter, Atmos. Environ., 115, 421–441, https://doi.org/10.1016/j.atmosenv.2014.08.072, 2015b.

IPCC: Climate change 2007: Synthesis Report. Contribution of Working Groups I, II and III to the Fourth Assessment Report of the Intergovernmental Panel on Climate Change, 2007.

IPCC: Climate change 2021: Synthesis Report. Contribution of Working Groups I, II and III to the Sixth Assessment Report of the Intergovernmental Panel on Climate Change., 2021.

Itahashi, S., Ge, B., Sato, K., Fu, J. S., Wang, X., Yamaji, K., Nagashima, T., Li, J., Kajino, M., and Liao, H.: MICS-Asia III: overview of model intercomparison and evaluation of acid deposition over Asia, Atmos. Chem. Phys., 20, 2667–2693, https://doi.org/10.5194/acp-20-2667-2020, 2020.

Jacobson, M. Z.: Developing, coupling, and applying a gas, aerosol, transport, and radiation model to study urban and regional air pollution, 1994.

Jacobson, M. Z.: Development and application of a new air pollution modeling system—Part III. Aerosol-phase simulations, Atmos. Environ., 31, 587–608, https://doi.org/10.1016/S1352-2310(96)00201-4, 1997.

Jacobson, M. Z.: Studying the effects of aerosols on vertical photolysis rate coefficient and temperature profiles over an urban airshed, J. Geophys. Res. Atmos., 103, 10593–10604, https://doi.org/10.1029/98jd00287, 1998.

Jacobson, M. Z.: GATOR-GCMM: A global-through urban-scale air pollution and weather forecast model: 1. Model design and treatment of subgrid soil, vegetation, roads, rooftops, water, sea ice, and snow, J. Geophys. Res. Atmos., 106, 5385–5401, https://doi.org/10.1029/2000JD900560, 2001.

Jacobson, M. Z.: Analysis of aerosol interactions with numerical techniques for solving coagulation, nucleation, condensation, dissolution, and reversible chemistry among multiple size distributions, J. Geophys. Res. Atmos., 107, AAC-2, https://doi.org/10.1029/2001JD002044, 2002.

Keita, S. A., Girard, E., Raut, J.-C., Leriche, M., Blanchet, J.-P., Pelon, J., Onishi, T., and Cirisan, A.: A new parameterization of ice heterogeneous nucleation coupled to aerosol chemistry in WRF-Chem model version 3.5.1: evaluation through ISDAC measurements, Geosci. Model Dev., 13, 5737–5755, https://doi.org/10.5194/gmd-13-5737-2020, 2020.

Klein, S. A., McCoy, R. B., Morrison, H., Ackerman, A. S., Avramov, A., Boer, G. de, Chen, M., Cole, J. N. S., Del Genio, A. D., and Falk, M.: Intercomparison of model simulations of mixed-phase clouds observed during the ARM Mixed-Phase Arctic Cloud Experiment. I: Single-layer cloud, Q. J. R. Meteorol. Soc. A J. Atmos. Sci. Appl. Meteorol. Phys. Oceanogr., 135, 979–

1002, https://doi.org/10.1002/qj.416, 2009.

Knote, C., Tuccella, P., Curci, G., Emmons, L., Orlando, J. J., Madronich, S., Baró, R., Jiménez-Guerrero, P., Luecken, D., and Hogrefe, C.: Influence of the choice of gas-phase mechanism on predictions of key gaseous pollutants during the AQMEII phase-2 intercomparison, Atmos. Environ., 115, 553–568, https://doi.org/10.1016/j.atmosenv.2014.11.066, 2015.

Kong, L., Tang, X., Zhu, J., Wang, Z., Fu, J. S., Wang, X., Itahashi, S., Yamaji, K., Nagashima, T., and Lee, H.-J.: Evaluation and uncertainty investigation of the NO_2, CO and NH_3 modeling over China under the framework of MICS-Asia III, Atmos. Chem. Phys., 20, 181–202, https://doi.org/10.5194/acp-20-181-2020, 2020.

Li, J., Nagashima, T., Kong, L., Ge, B., Yamaji, K., Fu, J. S., Wang, X., Fan, Q., Itahashi, S., and Hyo-Jung, L.: Model evaluation and intercomparison of surface-level ozone and relevant species in East Asia in the context of MICS-Asia Phase III–Part 1: Overview, Atmos. Chem. Phys., 19, 12993–13015, https://doi.org/10.5194/acp-19-12993-2019, 2019.

Li, M., Liu, H., Geng, G., Hong, C., Liu, F., Song, Y., Tong, D., Zheng, B., Cui, H., and Man, H.: Anthropogenic emission inventories in China: a review, Natl. Sci. Rev., 4, 834–866, https://doi.org/10.1093/nsr/nwx150, 2017.

Liu, Z., Wang, Y., Hu, B., Lu, K., Tang, G., Ji, D., Yang, X., Gao, W., Xie, Y., and Liu, J.: Elucidating the quantitative characterization of atmospheric oxidation capacity in Beijing, China, Sci. Total Environ., 771, 145306, https://doi.org/10.1016/j.scitotenv.2021.145306, 2021.

Ma, Y., Jin, Y., Zhang, M., Gong, W., Hong, J., Jin, S., Shi, Y., Zhang, Y., and Liu, B.: Aerosol optical properties of haze episodes in eastern China based on remote-sensing observations and WRF-Chem simulations, Sci. Total Environ., 757, 143784, https://doi.org/10.1016/j.scitotenv.2020.143784, 2021.

Mailler, S., Menut, L., Khvorostyanov, D., Valari, M., Couvidat, F., Siour, G., Turquety, S., Briant, R., Tuccella, P., and Bessagnet, B.: CHIMERE-2017: from urban to hemispheric chemistry-transport modeling, Geosci. Model Dev., 10, 2397–2423, https://doi.org/10.5194/gmd-10-2397-2017, 2017.

Makar, P. A., Gong, W., Milbrandt, J., Hogrefe, C., Zhang, Y., Curci, G., Žabkar, R., Im, U., Balzarini, A., Baró, R., Bianconi, R., Cheung, P., Forkel, R., Gravel, S., Hirtl, M., Honzak, L., Hou, A., Jiménez-Guerrero, P., Langer, M., Moran, M. D., Pabla, B., Pérez, J. L., Pirovano, G., San José, R., Tuccella, P., Werhahn, J., Zhang, J., and Galmarini, S.: Feedbacks between air pollution and weather, Part 1: Effects on weather, Atmos. Environ., 115, 442–469, https://doi.org/10.1016/j.atmosenv.2014.12.003, 2015a.

Makar, P. A., Gong, W., Hogrefe, C., Zhang, Y., Curci, G., Žabkar, R., Milbrandt, J., Im, U., Balzarini, A., Baró, R., Bianconi, R., Cheung, P., Forkel, R., Gravel, S., Hirtl, M., Honzak, L., Hou, A., Jiménez-Guerrero, P., Langer, M., Moran, M. D., Pabla, B., Pérez, J. L., Pirovano, G., San José, R., Tuccella, P., Werhahn, J., Zhang, J., and Galmarini, S.: Feedbacks between air pollution and weather, part 2: Effects on chemistry, Atmos. Environ., 115, 499–526, https://doi.org/10.1016/j.atmosenv.2014.10.021, 2015b.

Menut, L., Bessagnet, B., Khvorostyanov, D., Beekmann, M., Blond, N., Colette, A., Coll, I., Curci, G., Foret, G., and Hodzic, A.: CHIMERE 2013: a model for regional atmospheric composition modelling, Geosci. Model Dev., 6, 981–1028, https://doi.org/10.5194/gmd-6-981-2013, 2013.

Qu, Y., Voulgarakis, A., Wang, T., Kasoar, M., Wells, C., Yuan, C., Varma, S., and Mansfield, L.:

A study of the effect of aerosols on surface ozone through meteorology feedbacks over China, Atmos. Chem. Phys., 21, 5705–5718, https://doi.org/10.5194/acp-21-5705-2021, 2021.

Rosenfeld, D., Andreae, M. O., Asmi, A., Chin, M., de Leeuw, G., Donovan, D. P., Kahn, R., Kinne, S., Kivekäs, N., and Kulmala, M.: Global observations of aerosol-cloud-precipitation-climate interactions, Rev. Geophys., 52, 750–808, https://doi.org/10.1002/2013RG000441, 2014.

Safieddine, S., Boynard, A., Coheur, P.-F., Hurtmans, D., Pfister, G., Quennehen, B., Thomas, J. L., Raut, J.-C., Law, K. S., and Klimont, Z.: Summertime tropospheric ozone assessment over the Mediterranean region using the thermal infrared IASI/MetOp sounder and the WRF-Chem model, Atmos. Chem. Phys., 14, 10119–10131, https://doi.org/10.5194/acp-14-10119-2014, 2014.

Stein, O., Schultz, M. G., Bouarar, I., Clark, H., Huijnen, V., Gaudel, A., George, M., and Clerbaux, C.: On the wintertime low bias of Northern Hemisphere carbon monoxide found in global model simulations, Atmos. Chem. Phys., 14, 9295–9316, https://doi.org/10.5194/acp-14-9295-2014, 2014.

Tang, W., Yang, K., Qin, J., Li, X., and Niu, X.: A 16-year dataset (2000–2015) of high-resolution (3 h, 10 km) global surface solar radiation, Earth Syst. Sci. Data, 11, 1905–1915, https://doi.org/10.5194/essd-11-1905-2019, 2019.

Tuccella, P., Menut, L., Briant, R., Deroubaix, A., Khvorostyanov, D., Mailler, S., Siour, G., and Turquety, S.: Implementation of aerosol-cloud interaction within WRF-CHIMERE online coupled model: Evaluation and investigation of the indirect radiative effect from anthropogenic emission reduction on the Benelux Union, Atmosphere (Basel)., 10, https://doi.org/10.3390/atmos10010020, 2019.

Wallace, J. M. and Hobbs, P. V: Atmospheric science: an introductory survey, Elsevier, 2006.

Wang, K., Zhang, Y., Yahya, K., Wu, S.-Y., and Grell, G.: Implementation and initial application of new chemistry-aerosol options in WRF/Chem for simulating secondary organic aerosols and aerosol indirect effects for regional air quality, Atmos. Environ., 115, 716–732, https://doi.org/10.1016/j.atmosenv.2014.12.007, 2015.

Wang, K., Zhang, Y., Zhang, X., Fan, J., Leung, L. R., Zheng, B., Zhang, Q., and He, K.: Fine-scale application of WRF-CAM5 during a dust storm episode over East Asia: Sensitivity to grid resolutions and aerosol activation parameterizations, Atmos. Environ., 176, 1–20, https://doi.org/0.1016/j.atmosenv.2017.12.014, 2018.

Wang, K., Zhang, Y., Yu, S., Wong, D. C., Pleim, J., Mathur, R., Kelly, J. T., and Bell, M.: A comparative study of two-way and offline coupled WRF v3.4 and CMAQ v5.0.2 over the contiguous US: performance evaluation and impacts of chemistry–meteorology feedbacks on air quality, Geosci. Model Dev., 14, 7189–7221, https://doi.org/10.5194/gmd-14-7189-2021, 2021.

Wang, K., Gao, C., Wu, K., Liu, K., Wang, H., Dan, M., Ji, X., and Tong, Q.: ISAT v2. 0: an integrated tool for nested-domain configurations and model-ready emission inventories for WRF-AQM, Geosci. Model Dev., 16, 1961–1973, https://doi.org/10.5194/gmd-16-1961-2023, 2023.

Wang, S. and Hao, J.: Air quality management in China: Issues, challenges, and options, J. Environ. Sci., 24, 2–13, https://doi.org/10.1016/S1001-0742(11)60724-9, 2012.

Wang, Z., Wang, Z., Li, J., Zheng, H., Yan, P., and Li, J.: Development of a meteorology-chemistry two-way coupled numerical model (WRF-NAQPMS) and its application in a severe autumn haze simulation over the Beijing-Tianjin-Hebei area, China. Clim, Environ. Res, 19, 153–163, https://doi.org/10.3878/j.issn.1006-9585.2014.13231, 2014.

Wiedinmyer, C., Akagi, S. K., Yokelson, R. J., Emmons, L. K., Al-Saadi, J. A., Orlando, J. J., and Soja, A. J.: The Fire INventory from NCAR (FINN): A high resolution global model to estimate the emissions from open burning, Geosci. Model Dev., 4, 625–641, https://doi.org/10.5194/gmd-4-625-2011, 2011.

Wong, D. C., Pleim, J., Mathur, R., Binkowski, F., Otte, T., Gilliam, R., Pouliot, G., Xiu, A., Young, J. O., and Kang, D.: WRF-CMAQ two-way coupled system with aerosol feedback: software development and preliminary results, Geosci. Model Dev., 5, 299–312, https://doi.org/10.5194/gmd-5-299-2012, 2012.

Xing, J., Mathur, R., Pleim, J., Hogrefe, C., Wang, J., Gan, C.-M., Sarwar, G., Wong, D. C., and McKeen, S.: Representing the effects of stratosphere–troposphere exchange on 3-D O_3 distributions in chemistry transport models using a potential vorticity-based parameterization, Atmos. Chem. Phys., 16, 10865–10877, https://doi.org/10.5194/acp-16-10865-2016, 2016.

Xing, J., Wang, J., Mathur, R., Wang, S., Sarwar, G., Pleim, J., Hogrefe, C., Zhang, Y., Jiang, J., and Wong, D. C.: Impacts of aerosol direct effects on tropospheric ozone through changes in atmospheric dynamics and photolysis rates, Atmos. Chem. Phys., 17, 9869–9883, https://doi.org/10.5194/acp-17-9869-2017, 2017.

Xu, K.-M. and Randall, D. A.: A semiempirical cloudiness parameterization for use in climate models, J. Atmos. Sci., 53, 3084–3102, https://doi.org/10.1175/1520-0469(1996)053<3084:ASCPFU>2.0.CO;2, 1996.

Zaveri, R. A., Easter, R. C., Fast, J. D., and Peters, L. K.: Model for simulating aerosol interactions and chemistry (MOSAIC), J. Geophys. Res. Atmos., 113, https://doi.org/10.1029/2007JD008782, 2008.

Zhang, X., Wu, Y., Liu, X., Reis, S., Jin, J., Dragosits, U., Van Damme, M., Clarisse, L., Whitburn, S., and Coheur, P.-F.: Ammonia emissions may be substantially underestimated in China, Environ. Sci. Technol., 51, 12089–12096, https://doi.org/10.1021/acs.est.7b02171, 2017.

Zhang, Y.: Online-coupled meteorology and chemistry models: history, current status, and outlook, Atmos. Chem. Phys, 8, 2895–2932, https://doi.org/10.5194/acp-8-2895-2008, 2008.

Zhang, Y., Zhang, X., Wang, K., Zhang, Q., Duan, F., and He, K.: Application of WRF/Chem over East Asia: Part II. Model improvement and sensitivity simulations, Atmos. Environ., 124, 301–320, https://doi.org/10.1016/j.atmosenv.2015.07.023, 2016.

Zhao, B., Liou, K., Gu, Y., Li, Q., Jiang, J. H., Su, H., He, C., Tseng, H.-L. R., Wang, S., and Liu, R.: Enhanced PM2.5 pollution in China due to aerosol-cloud interactions, Sci. Rep., 7, 1–11, https://doi.org/10.1038/s41598-017-04096-8, 2017.

Zhou, C., Zhang, X., Gong, S., Wang, Y., and Xue, M.: Improving aerosol interaction with clouds and precipitation in a regional chemical weather modeling system, 16, 145–160, https://doi.org/10.5194/acp-16-145-2016, 2016.

Zhu, J., Wang, S., Wang, H., Jing, S., Lou, S., Saiz-Lopez, A., and Zhou, B.: Observationally constrained modeling of atmospheric oxidation capacity and photochemical reactivity in Shanghai, China, Atmos. Chem. Phys., 20, 1217–1232, https://doi.org/10.5194/acp-20-1217-2020, 2020.

Zhu, J., Chen, L., Liao, H., Yang, H., Yang, Y., and Yue, X.: Enhanced $PM_{2.5}$ decreases and O_3 increases in China during COVID-19 lockdown by aerosol-radiation feedback, Geophys. Res.

Lett., 48, 1–11, https://doi.org/10.1029/2020GL090260, 2021.